Potential influence of landscape transition on stream water chemistry trends during the last decades in a karst catchment (Pyrenees, SW France) in a context of global environmental changes

F. Ulloa-Cedamanos, J.L. Probst, C. Marais-Sicre, E. Vrech, Eric Maire, Anne Probst

Ecological Indicators 140 (2022) 109023

Contents lists available at ScienceDirect

Ecological Indicators

journal homepage: www.elsevier.com/locate/ecolind

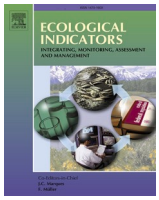

Original Articles

Potential influence of landscape transition on stream water chemistry trends during the last decades in a karst catchment (Pyrenees, SW France) in a context of global environmental changes

F. Ulloa-Cedamanos [a,d,e,*], J.L. Probst [a,d,e], C. Marais-Sicre [b,e], E. Vrech [a,d,e], E. Maire [c,e], A. Probst [a,d,e,*]

[a] Laboratoire Ecologie fonctionnelle et Environnement, Université de Toulouse, CNRS, 31326 Castanet Tolosan, France
[b] Centre d'Etudes Spatiales de la Biosphère, Université de Toulouse, CNES, CNRS, IRD, INRA, UT3 Paul Sabatier, 31400 Toulouse, France
[c] Géographie de l'Environnement, Université de Toulouse, CNRS, UT2 Jean Jaurès, 31058 Toulouse, France
[d] LTER Bassin versant du Baget, SNO Karst, IR OZCAR, CNRS, University of Toulouse, France
[e] LTSER Zone Atelier Pyrénées-Garonne, CNRS, University of Toulouse, France

ARTICLE INFO

Keywords:
Landscape indicator
Hydrochemical indicator
Chemical weathering
Long-term trends
Climate change
Acid deposition
Remote sensing
Pyrenees mountains

ABSTRACT

Over the last century, lands used for livestock and agriculture have been progressively abandoned on mountains across Europe. The afforestation of abandoned agricultural lands leads to significant environmental impacts particularly in karst catchments, which are highly responsive to climate change and human disturbances. Due to the lack of long-term historical records and appropriate methods, these impacts are not yet well investigated. The remote Baget forested catchment (Pyrenees Mountains), where a long-term hydrochemical survey has been conducted since 1979, was chosen to develop a method for reconstructing the evolution of landscapes based on heterogeneous and multi-temporal satellite imagery and aerial photographs from 1942 onwards. An indicator of landscape change is proposed, based on three vegetation groups, compatible with the various supporting data. The spatio-temporal landscape evolution evidenced a regular increase of 31% in forest extension between 1942 and 2019, while pioneer (grassland and heathlands) and open forest (early woodland) stages showed an overall but uneven decrease, marked by an accelerated decline of the latter due to an increase in livestock activities. The trends of streamwater discharge and chemistry were related to these environmental changes. A set of processes influencing the changes in the hydrochemical patterns, particularly the increase in dissolved elements in streamwater originating from carbonate dissolution, is proposed and discussed. The forest recolonization (+0.05 $Km^2.yr^{-1}$) enhanced soil organic matter content, generating an increased pCO_2 in soils, which in turn enhanced the carbonate dissolution, expressed by a concentration increase of + 5 $\mu eq.L^{-1}.yr^{-1}$ for (Ca^{2+}+Mg^{2+}) and of + 10 $\mu eq.L^{-1}.yr^{-1}$ for HCO_3^-. The steeper slope of HCO_3^- could result from decreasing terrestrial Ca^{2+}+Mg^{2+} export together with decreasing SO_4^{2-} leaching (−4 $\mu eq.L^{-1}.yr^{-1}$) due to decreasing acid atmospheric deposition. In the meantime, the observed increase in air temperature (+0.03 °C.yr^{-1}) favoured tree growth, litter decomposition and water demand by trees. This study has demonstrated the powerful indicator of linking the historical evolution of the landscape, quantified using images, to the observed trends in the hydrochemical composition of stream waters, to highlight the internal processes of the critical zone. However, because of nested effects, it still remains a challenge to strictly quantify their respective impact on streamwater chemistry.

1. Introduction

Mountainous karst hydrosystems are critical zones that are sensitive to climatic variations and anthropogenic pressures (IPCC, 2014; López-Moreno et al., 2014; Morán-Tejeda et al., 2010). Consequently, the Karstic Critical Zone (K-CZ) is an excellent model for studying their impacts on water resources and on the biogeochemical cycles of carbon and nitrogen, currently greatly disturbed by land use changes. Karst environments display marked geomorphological characteristics, involving surface discontinuities and a complex network of water

* Corresponding authors at: Laboratoire Ecologie fonctionnelle et Environnement, Université de Toulouse, CNRS, 31326 Castanet Tolosan, France.
E-mail addresses: francesco.ulloa-cedamanos@umontpellier.fr (F. Ulloa-Cedamanos), anne.probst@toulouse-inp.fr (A. Probst).

https://doi.org/10.1016/j.ecolind.2022.109023
Received 23 March 2022; Received in revised form 25 May 2022; Accepted 28 May 2022
Available online 4 June 2022

pathways, which connect surface water to groundwater (Bakalowicz, 2005, 1979; Daher et al., 2011). This proximity between the two types of waters results in water mixing leading to a high vulnerability of the water resource, as anthropogenic contaminants can rapidly reach the groundwater. Moreover, the dissolution of carbonates, the main lithology forming karst systems, is very sensitive to climate changes. Climate warming increases pCO_2 in soils by promoting the activity of microorganisms and the mineralization of organic matter (Deines, 1980; Li et al., 2010). Consequently, this leads to a variation in weathering products and the physico-chemical characteristics of stream and ground waters (Binet et al., 2020).

The modernization of agriculture in the second half of the 20th century led to the abandonment of less productive lands and less accessible areas (Chassany, 1999). From this period onwards, a rural exodus, especially in mountainous areas, accompanied the sharp decline in pastoralism and agricultural land use (Camacho et al., 2008). The abandonment led to a progressive forest recolonization (Pointereau and Coulon, 2009) through vegetation transition to the forested state (Génot and Schnitzler, 2012; Rameau, 1999). Forests are a key factor in the carbon cycle through their role as a carbon sink through photosynthesis that fixes atmospheric carbon (the inverse of Equation (1)). They also act as a carbon source to the atmosphere via autotrophic respiration and indirectly via the contribution of organic matter to the soil (above and below ground litter, root exudates), where they are decomposed by microorganisms (Catalán et al., 2016; Clark and Fritz, 1997; Porcal et al., 2015; Reynolds et al., 2017). The recolonization by forests of land abandoned after agricultural activities therefore promotes the production of organic matter in the soil (Arrouays et al., 2001). These changes can lead to an increase in the partial pressure of CO_2 (pCO_2) in the soils and in the karstic networks (Equation (1)) (Raich and Tufekcioglu, 2000; Rasse et al., 2001). This increase can favour the dissolution of carbonates (Equations (2) and (3)) and the hydrolysis of silicate minerals (Cao et al., 2019; Hartmann et al., 2009; Moquet et al., 2011), but may also enhance the production of dissolved organic carbon (DOC) in the water. Thus, landscape transition is a potential indicator of modifications in the carbon fluxes through changes in chemical weathering in the K-CZ.

$$CH_2O + O_2 \rightarrow CO_2 + H_2O, \quad (1)$$

Natural drivers (i.e., climate, soil type, vegetation and organic matter inputs) and anthropogenic activities influence the carbon fluxes between the atmosphere and the soils. In the K-CZ, the natural parameters controlling the dissolution of carbonates (Equations (2) and (3)), and consequently the water chemistry are the plant species and the soil properties (Calmels et al., 2014). These are directly affected by temperature, precipitation and age since deglaciation, which all change differently with elevation in different mountain areas (Theurillat and Guisan, 2001). Plant species influence the quantity and characteristics of organic matter, affecting their decomposition by microorganisms and the CO_2 production in the soils (Equation (1)). For instance, the rate of natural carbonate weathering in the Jura Mountains is 20–30% higher under deciduous than under coniferous vegetation (Calmels et al., 2014).

$$CO_2 + H_2O \rightarrow H_2CO_3, \quad (2)$$

$$CaCO_3(calcite) + H_2CO_3 \leftrightarrow Ca^{2+} + 2HCO_3^-, \quad (3)$$

Thanks to advances in remote sensing, the availability and improved spatial resolution of satellite imagery on the one hand, and the availability of ancient aerial photographs on the other hand, land use changes can be analysed over large areas and over long time periods (Dusseux, 2014; Guerschman et al., 2003). These tools facilitate a regular monitoring of natural phenomena and indicators on the Earth's surface (Sawadogo et al., 2008) such as vegetation dynamics and changes in the land cover (Girard and Girard, 2010). However, it remains challenging to converge these products in a harmonized way.

Over the world, some studies have shown a significant long-term (>10–30 years) change in the chemical composition of stream waters. Changes in various environmental parameters were pointed out such as air temperature (Ulloa-Cedamanos et al., 2020), atmospheric acid deposition (Binet et al., 2020; Pierret et al., 2018; Vuorenmaa et al., 2018), agricultural activities (Stets et al., 2014), rainfall (Yan et al., 2011) and even a potential role of the dominant type of land cover (Raymond and Cole, 2003). Meanwhile, an increase in the partial pressure of CO_2 (pCO_2) has been highlighted in karst cavities and soils, in Belgian (Ek and Godissart, 2014), Swedish and French catchments (Jeannin et al., 2016). It has been suggested that this rise in pCO_2 is linked to an increase of about 30% of the forest in thirty years (Ek and Godissart, 2014), or to changes in agricultural practices and global warming (Jeannin et al., 2016). In addition, obvious changes in land use mainly due to farmland abandonment were observed in Europe (García-Ruiz and Lana-Renault, 2011; Rabbinge and van Diepen, 2000), including the Pyrenees mountains (Houet et al., 2012, López-Moreno et al., 2014). In this region, forest recolonization (García-Ruiz et al., 2011; López-Moreno et al., 2011) and global warming (López-Moreno et al., 2014; Amblar-Francés et al., 2020) have led to a decline in water availability. Despite these studies, while trends have been observed, the connection between the changes in land use and the trends in stream water chemistry on the long-term, has seldom been investigated and quantified in remote areas. The reason is the lack of long-term hydrochemical historical records over decades and of appropriate methods to harmonize data from recent satellite imagery and ancient aerial photographs.

In this context, the Baget karstic catchment (BC) was selected as a pilot site, because a complete set of hydrochemical data covering almost 50 years was available. The objectives of this study were as follows: (i) to develop and apply a method for reconstructing the evolution of the landscape in the BC over decades using satellite imagery and aerial photographs from 1942 onwards, (ii) to confront the indicators of land cover change with the evolution of the stream discharge and stream-water chemistry in this sensitive K-CZ, and (iii) to decipher the influence of changes in the environmental parameters on the water chemical trends.

The supporting hypothesis was that the progressive expansion of the forest area in the BC would imply, with a time shift, an enhancement of the biogeochemical cycles in the soils, and then, would affect the stream hydrochemical patterns. This amplification would lead to an increase in pCO_2 within the soil-rock system and thus stimulate chemical weathering processes, and control the changes in the water chemistry. At the same time, other key environmental pressure factors linked to global warming could antinomically accelerate/moderate these changes.

2. Materials and methods

2.1. Description of the study area

The Baget catchment (BC, centroid in 42°57′42″ N, 0°58′30″ E) is a small karstic and forested basin with a surface area of 13.25 km^2 (Fig. 1; Bakalowicz, 1979; Labat et al., 2000; Ulloa-Cedamanos et al., 2020). The BC is located in the lower part of the Pyrenees, in southwestern France. Its altitude ranges from 498 (elevation outlet) to 1417 m, with very steep slopes, particularly in the middle part of the basin where they reach up to 60% (Mangin, 1975).

The BC exhibits an Atlantic oceanic climate with a clear mountainous influence. The average rainfall and evapotranspiration are respectively 1700 mm and 540 mm (Johannet et al., 2008; Mangin, 1975; Padilla et al., 1994). The annual average daily air temperature is 11.8 ± 6.3 °C for the period between 1961 and 2020, recorded at the nearest meteorological station of Saint Girons (43°00′19″ N, 1°06′25″ E, altitude 414 m, operated by Météo France) about 8.3 km from the outlet of the BC (Ulloa-Cedamanos et al., 2020). Between October 2019 and September 2020, 60% of annual precipitation (1713 $mm.yr^{-1}$) occurred from November to December, and March to May (wet seasons) (Ulloa-

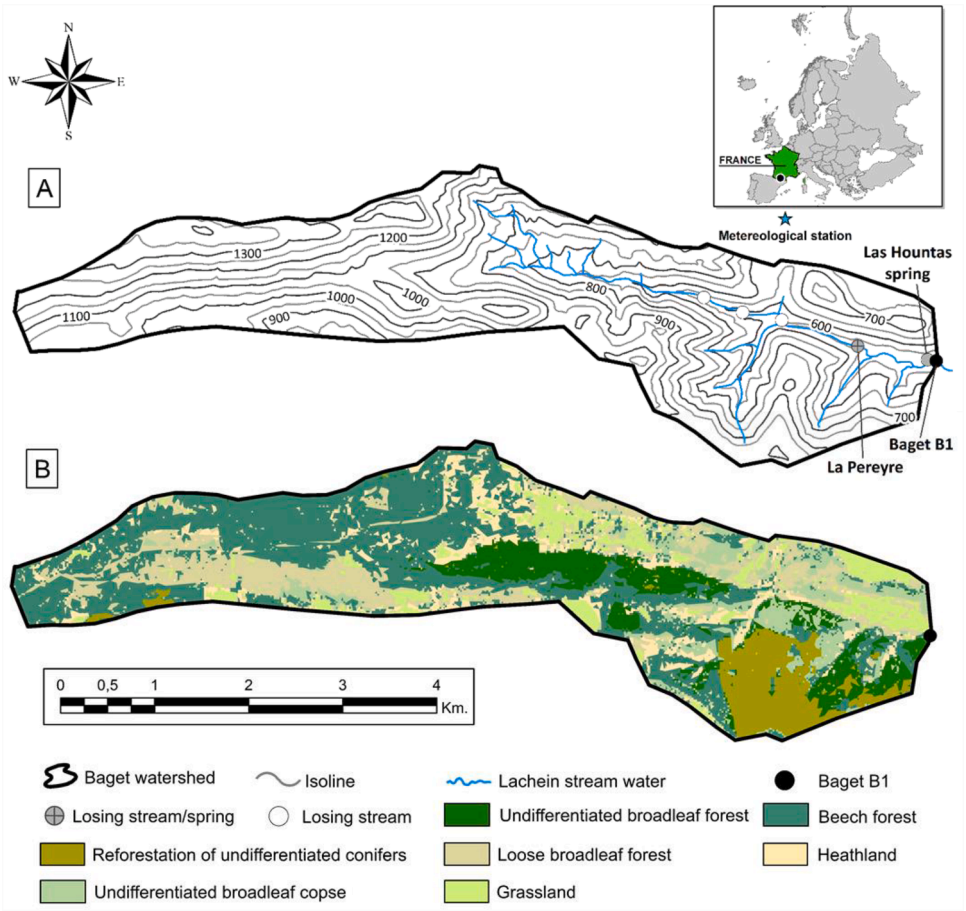

Fig. 1. (A) Location and relief with contour lines (in meters) and (B) land cover of the Baget catchment (BC) in 2019. Modified from Ulloa-Cedamanos et al. (2021a). The coordinates of the extreme edges of BC are 42°58′21.9″ N, 0°58′15.9″ E (north), 42°56′41.1″ N, 1°0′21.3″ E (south), 42°57′19.9″ N, 1°1′52.1″ E (east) and 42°57′27.7″ N, 0°54′40.5″ E (west).

Cedamanos et al., 2021a). The main stream is oriented west to east. The average annual discharge is 0.48 $m^3.s^{-1}$ (i.e., a specific flow of 36 $L.s^{-1}.km^{-2}$, between 1970 and 1997, Labat et al., 2000) at the outlet (Baget B1, Fig. 1). Recent studies report in BC an average discharge of 0.44 ± 0.67 $m^3.s^{-1}$, with extreme values of 10.10 and 0.02 $m^3.s^{-1}$ for the period 1979 to 2018 (Ulloa-Cedamanos et al., 2020). The period of high-water flow occurs from November to May, and is controlled by a bimodal rainfall regime with generally a first peak at the beginning of winter in December and a second peak in late spring in May. Approximately 50% of the total streamflow occurs between December and March (Mangin, 1975; Ulloa-Cedamanos et al., 2020).

From 1970 onwards, rural abandonment and the ageing agricultural population led to an agricultural and pastoral decline in this region (Barrué-Pastor and Fournié, 1996). The consequences are perceptible with the progressive forest recolonization, and the sparsity of livestock farms in this area dedicated to breeding. The BC is mainly wooded (67% of the catchment surface, Fig. 1B). A dense mixed deciduous and coniferous forest dominates the upper basin (above 900 m, Fig. 1A), while grasslands are observed on the south-facing slope and near the outlet (Ulloa-Cedamanos et al., 2020). Livestock are present in the grasslands (about 250 animals), while herds are only present from May to November.

This catchment drains a large carbonate area (67% of total surface; Mangin, 1975; Ulloa-Cedamanos et al., 2021b) with 98% calcite dating from the Jurassic and Lower Cretaceous (Debroas, 2009; Mangin, 1975). It is clearly distinguished from other karst systems in the region by a high specific dissolution of carbonates (Bakalowicz, 1979), which leads to the dominance of some ions, as shown by the discharge-weighted mean concentrations for calcium (Ca^{2+}, 2.97 ± 0.18 $meq.L^{-1}$) and for bicarbonate (HCO_3^-, 2.90 ± 0.22 $meq.L^{-1}$) in surface water, as observed in BC for the period 1979–2018. The weathering of secondary lithologies in BC provides other less abundant major elements such as magnesium (Mg^{2+}, 0.36 ± 0.05 $meq.L^{-1}$, 1979–2018) and sulphate (SO_4^{2-}, 0.35 ± 0.13 $meq.L^{-1}$, 1995–2018). The other major elements (sodium–Na^+, chloride–Cl^-, nitrate–NO_3^- and potassium–K^+) from atmospheric or biological origin, display concentrations of<0.05 $meq.L^{-1}$ (Ulloa-Cedamanos et al., 2020). According to Ulloa-Cedamanos et al. (2021b), the contribution of mineral/rock weathering to streamwater chemistry at the outlet is as follows: pyrite oxidation (1% of the total dissolved solids, called TDS) < carbonate dissolution by sulfuric acid (3%) ≈ gypsum dissolution (3%) ≪ silicate weathering by carbonic acid (16%) ≪ carbonate dissolution by carbonic acid (73%).

2.2. Hydrochemical survey

The BC was monitored at the outlet (Baget B1, Fig. 1) between 1979 and 2020. The outlet represents the integration of the whole catchment in terms of response to environmental factors. The monitoring frequency was as follows: a weekly frequency from 1979 to 2006 by the CNRS (French National Centre for Scientific Research) laboratory of Moulis (Binet et al., 2020), a biannual frequency by the BRGM (Bureau de Recherches Géologiques et Minières) Occitanie (ADES database, 2021) from 2007 to 2014, and a bi-monthly frequency between October 2016 and September 2020 by the Laboratory of Functional Ecology and Environment (Ulloa-Cedamanos et al., 2020).

Rainfall was measured from September 2019 to December 2020 at

the meteorological station of Balagué nearby BC (42°58′06.5″ N 1°00′39″ E, elevation 658 m, Fig. 1A). Rainfall between September 1978 and August 2019 was calculated using the very significant relationship ($R^2 = 0.80$; $p < 0.001$; $n = 365$, with a slope of 1.39) between the daily rainfall registered at Balagué station and at the closest Météo-France meteorological station of St. Girons (elevation 414 m, situated 8.3 km downstream from the outlet of BC) (Ulloa-Cedamanos et al., 2021a). Daily temperature and daily potential evapotranspiration (ETP model, Penman-Monteith method) were also recorded at the same Météo-France meteorological station. A strong correlation was observed between these two parameters for the period October 1978 - September 2018 ($R^2 = 0.70$; $p < 0.001$; $n = 14604$, with a slope of 3.7).

The discharge (Q, $m^3.s^{-1}$) of the Lachein stream was acquired from the water level data measured at the monitoring station located at Baget B1 (Fig. 1). This site is equipped with a mechanical limnigraph (OTT 20 1/5, Loveland, CO, USA) and a float-type water level sensor (OTT Thalimedes, Loveland, CO, USA). The water height data (H), freely accessible since 1968 (Banque Hydro, 2021), were transformed into Q from a rating curve H/Q plot (Mangin, 1975; Ulloa-Cedamanos et al., 2021a).

The physico-chemical parameters including pH, conductivity (in µS. cm^{-1}) and water temperature (in °C) were measured with a multi-parameter probe (ProfiLine Multi 3320, WTW, Xylem Analytics Germany Sales GmbH & Co., Weilheim, Germany) directly in the stream during sampling at the outlet (Fig. 1). Water samples were collected in a 1 L HDPE bottle and stored in darkness at 5 °C until analyses. Prior to analyses, all samples were filtered through 0.22 µm Millipore cellulose nitrate membranes. Alkalinity was measured using a standard acid titration method with 0.02 N HCl and a Metrohm titrant (716 DMS Titrino, Metrohm, Riverview, Florida, USA). Strong acid anion concentrations (SO_4^{2-}, NO_3^- and Cl^-) were measured by ion chromatography (Dionex apparatus ICS 5000+, Thermo Fisher Scientific, Waltham, MA, USA). Samples were previously acidified with 16 N HNO_3 and analysed for major cation (Ca^{2+}, Mg^{2+}, Na^+ and K^+) and silica concentrations by an inductively coupled plasma optical emission spectrometer (ICP-OES; Iris Intrepid II XLD, Thermo Electron, Thermo Fisher Scientific, Waltham, MA, USA). The TDS (total dissolved solids, $mg.L^{-1}$) is the sum of the major elements (Ca^{2+}, Mg^{2+}, Na^+, K^+, HCO_3^-, SO_4^{2-}, NO_3^-, Cl^- and H_4SiO_4). Protons and ammonium (NH_4^+) were negligible in our case study. The Net Inorganic Charge Balance (NICB = 200 × (TZ^+ - TZ^-)/(TZ^+ + TZ^-), in %) between the sum of cations (TZ^+) and the sum of anions (TZ^-) (considered both in $meq.L^{-1}$) was within a ± 10% range for 99.5% of samples.

Regarding the quality assurance (QA) and the quality control (QC), the data set was too long to have a QA/QC procedure over the entire period from 1978 until 2020. Concerning the QA, the protocols for the sampling, filtration, pre-treatment, and storage of the streamwater before analysis were controlled during the entire period. In relation to the QC, all the methods of analysis were controlled following French (NF), European (EN), and international (ISO) standards. Moreover, for several decades, the physico-chemical analysis platform of the Laboratoire écologie fonctionnelle et environnement has participated each year in the ICP-Water Intercomparison protocol lead by the Norwegian Institute for Water Research (NIVA), which follows a QA/QC procedure.

2.3. Landscape classification

A synthetic flow chart of the methodological approach is presented in Appendix A. All the landscape classification procedure was performed in QGIS software (QGIS Development Team, 2021).

2.3.1. Input imagery data

We reconstructed the evolution of land cover since 1942 (the oldest aerial photograph available in the basin, Appendix B Figure B.1), at 8-year intervals, except for the period 1947–1963 due to missing data (Fig. 2). The time step of 8 years was chosen since the impact of changes in land cover was not detected for a lower time-step on water chemistry, and also to match with the availability of the supporting data. The following data (Appendix B Table B.1) were used as input of the model:

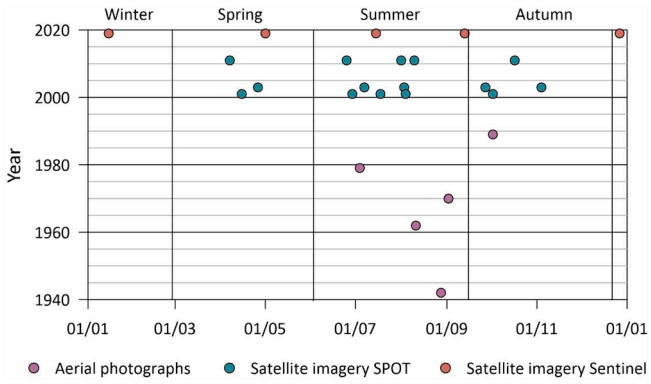

Fig. 2. Temporal distribution of the available dataset images over the year for the period 1940–2020. The resolution of sentinel-2 is 10 m, that of SPOT-2 and 4 is between 10 and 20 m.

(i) Satellite imagery SPOT 2 and 4 (between 2001 and 2011) and Sentinel 2 (since 2015) (available on the Theia-Land platform),
(ii) Aerial photographs between 1942 and 1989 available on the IGN (National Institute for Geographic and Forestry Information) website and,
(iii) Exogenous data for the recognition of the site, including images in Google Earth, Forest Inventory and digital elevation model raster (DEM). The last two data sets are available on the IGN website.

2.3.2. Data processing

The processing of aerial photographs, unlike satellite imagery, requires pre-processing including *ortho*-rectification, geo-referencing and inclusion of Digital Elevation Model (DEM) data. Considering the information provided by the aerial photographs, a texture index was included via the texture ratio (Haralick et al., 1973; Huang et al., 2007), in complement to the pixel values. The main disadvantages of the aerial photographs were: (i) the irregularity of acquisition campaigns mainly carried out between May and October due to meteorological constraints, (ii) the one-off availability of photographs per year, and (iii) the cover of the surface catchment by several image mosaics (Fig. 2, Appendix A, Appendix B Figure B.1). For the satellite images, the challenge was to select five images at different dates without a dense cloud cover, representing the main seasons of the year. The set of images for each year was aggregated to obtain a multi-temporal yearly image containing a large number of bands suitable for land cover detection of the whole catchment area.

2.3.3. Processing and exploitation of imagery data

Multi-temporal images and multi-source data have already been used to study changes in land cover (Dusseux, 2014) for assessing various environmental processes (Grinand et al., 2013), such as the influence of ancient ecological processes on current biodiversity (Herrault, 2015).

The photo-interpretation of imagery data (Google Earth) and the IGN forest inventory of 1987 served to develop the nomenclature (Miranda et al., 2018) and to identify the tree species, as well as the location of anthropic structures (buildings, roads, cultivated areas). These data constitute the training dataset, 50% of which was used in the classification model and the other half to validate the classification image (Marais Sicre et al., 2020). This step was crucial, as the quality of class equality, maximum intra-class homogeneity and inter-class heterogeneity determine the pixels classification and therefore the discrimination of the different classes.

The method used was a supervised classification fed by the first half of the training dataset using the Orfeo Toolbox in QGIS software (QGIS Development Team, 2021). This process treats each pixel one by one from the image provided using the Random Forest algorithm (Breiman, 2001; Marais Sicre et al., 2020), in order to assign all pixels to a certain class. This non-parametric algorithm (Breiman, 2001) was used due to the better performance compared to other classification algorithms (Gislason et al., 2006), its robustness in wide area classification (Pelletier et al., 2017) and the easy parameterization (Rodriguez-Galiano et al., 2012). Thus, seven main land cover types were identified over the whole basin (Fig. 1, Appendix C) using satellite images, with beech and broadleaf forests as the two dominant land covers. However, the use of only one date per year (Fig. 2) and the quality of the old aerial photographs impeded the classification into seven classes. Aiming for a common indicator of landscape change, applicable to both satellite images and aerial photos, we selected a landscape classification including three main vegetation transitions: pioneer, open forest and mature forest stage (Table 1) (§ Appendix C for more details). This classification took into account the land cover transition, the biomass density and the potential influence over pCO_2 production in soils. Each resulting raster with the landscape classification was transformed into a polygon (polygonise tool) to quantify the surface area of each type of landcover.

2.3.4. Evaluation of the classified image

The land cover classification was assessed using the F-score (Powers, 2011; Van Rijsbergen, 1979), the kappa index (Marais Sicre et al., 2020) and the confusion matrix (Congalton, 1991). The F-score is the harmonic mean of each class, i.e., an average between the precision (number of correctly classified pixels among all classified pixels) and the sensitivity (number of classified pixels over correctly classified pixels, for each class). Thus, the F-score quantifies the proportion of well-classified pixels of each class. The kappa index is the relative difference between the proportion of agreement observed and the proportion of random agreement for the whole model (Marais Sicre et al., 2020). The land cover reconstruction also generates a confusion matrix to assess the robustness of the classification. Confusion matrix shows which classes were confused with each other, i.e., which pixels were classified in the wrong classes.

For the classifications generated on aerial photographs, the evaluation was carried out on each mosaic and then averaged over all the mosaics covering the catchment. For satellite images, the assessment was carried out on the classified and smoothed image (use of a majority filter (3x3) to discard isolated pixels). The evaluations were based on the second half of the training dataset.

2.4. Indicators of changes for landscape and water chemistry

In order to evaluate the intensity of the change in land cover (R), water chemistry (X) or discharge (Q), we calculated the rate of growth/decline of these parameters with reference to the year 1979 (Eqs. (4)–(6), Maaf-IGN, 2016), since water chemistry data were available from this year (see above § 2.2).

$$R(\%) = \frac{S_y - S_{1979}}{S_{1979}} \times 100 \quad (4)$$

$$X(\%) = \frac{C_y - C_{1979}}{C_{1979}} \times 100 \quad (5)$$

$$Q(\%) = \frac{Q_y - Q_{1979}}{Q_{1979}} \times 100 \quad (6)$$

where S_y, C_y and Q_y are the surface of each land type, average concentrations and discharge at year-step y, respectively. The S_{1979}, C_{1979}, and Q_{1979} correspond to values of the surface of each land type, concentrations and discharge in 1979.

The average concentration (C) of each element for each year was weighted by discharge (Q), according to the following equation (Littlewood, 1995; Phillips et al., 1999):

$$C\left(meq.L^{-1}\right) = \frac{\sum_i^n (C_i * Q_i)}{\sum_i^n (Q_i)} \quad (7)$$

The loss of alkalinity (in equivalent %) was calculated as follows for carbonated systems (Perrin et al., 2008; Ulloa-Cedamanos et al., 2020):

$$\Delta Alk = \frac{\left(Ca^{2+} + Mg^{2+}\right) - HCO_3^-}{\left(Ca^{2+} + Mg^{2+}\right)} \times 100 \quad (8)$$

2.5. Statistical analysis

All calculations were computed on a hydrological year basis (October–September). For simplicity, only the second year of each period will be indicated, for example the period from October 1978 to September 1979 will be named as the year 1979. Statistical data processing was performed in R (R Core Team, 2021) using RStudio software (RStudio Team, 2020). Redundancy analysis (RDA, Jari Oksanen et al., 2020) is a two-step analysis in which individual and environmental data are analysed using multivariate linear regression, producing a matrix of fitted values. Then, PCA of the fitted values was used to produce canonical axes, which were linear combinations of the predictors (Legendre and Legendre, 2012). RDA was used to analyse many individual characteristics and environmental predictors simultaneously (Forester et al., 2018). This technique has been widely used in ecology to assess the cause-effect relationship between changes in the genotype or phenotype of individuals and fluctuations in environmental factors (Forester et al., 2018; Jalal et al., 2005). The linear regression (R Core Team, 2021) was used to determine the long-term trend of each parameter, together with the significance level (p-value) and the Spearman correlation coefficient (R^2).

Table 1
Usage of terms.

Term	Usage
Vegetation transition	A process of change in the vegetation communities over time from pioneer to forest stage.
Pioneer community stage	A community of heaths and grasses developed on an abandoned field, formerly used for agriculture or livestock farming.
Open forest stage	A seral community in the early stages of forest transition. It includes loose forest and broadleaf copse.
Mature forest stage	A steady forest ecosystem reached through the process of vegetation transition. The forest communities encompass stands of broadleaf and coniferous trees.

3. Results

3.1. Reconstructing the evolution of landscapes

The Baget catchment landscape was mapped based on the classification set up in section 2.3, to study the evolution of the landscape from 1942 to 2019 (Fig. 3).

The overall performances (kappa index) of the aerial photographs were 0.54 (Fig. 4A). The mature forest stage was the class with the highest F-score (mean of 0.80), while the open forest stage had the lowest F-score (mean of 0.50) (Appendix B Figure B.3). The lower index from 1979 to 1989 is due to the fact that the reconstituted images were sometimes made up of several mosaics (between 2 and 4) and were acquired at different periods of the year. The kappa index of the satellite image classifications was relatively stable (mean of 0.72) and higher than those generated for aerial photographs. However, the F-scores show that some groups were slightly misclassified (Fig. 4A). This is owing to the difficulty of identifying some types of land cover such as

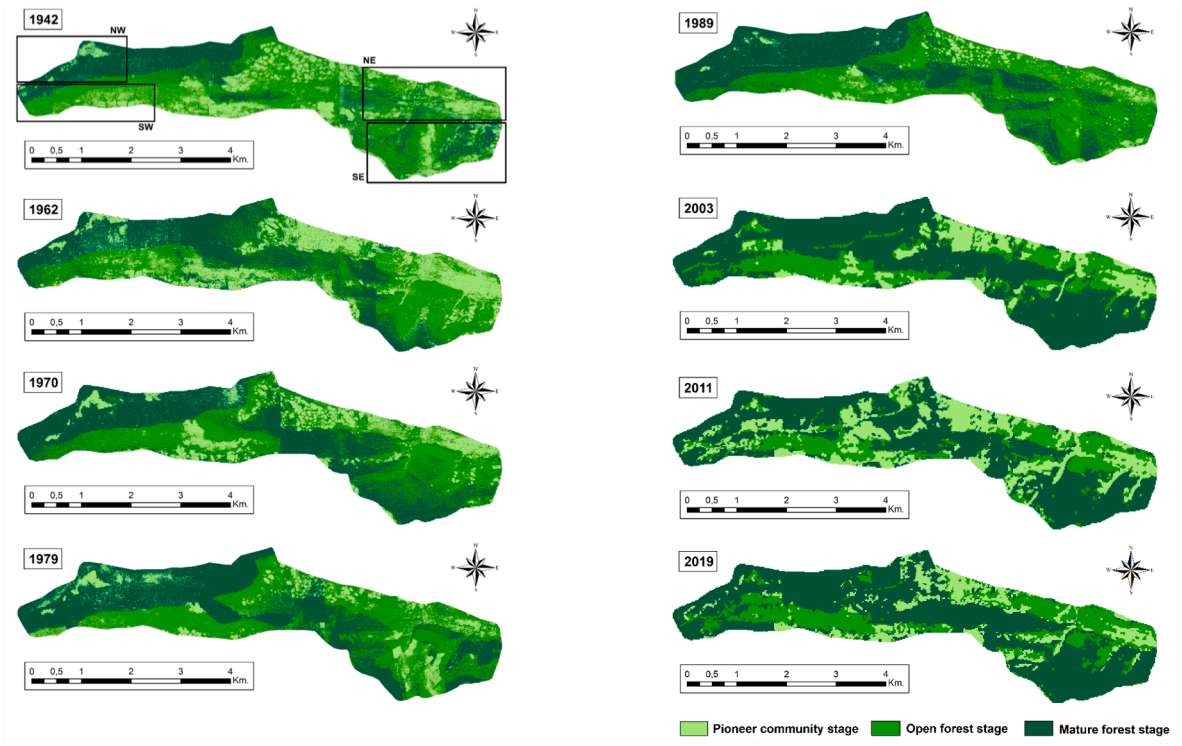

Fig. 3. Evolution of landscape in the Baget catchment from 1942 to 2019. Data input: aerial photographs between 1942 and 1989, satellite imagery SPOT 2 and 4 (between 2001 and 2011), and sentinel 2 (since 2019). In the map of 1942, NW: Northwest, SW: Southwest, NE: Northeast, SE: Southeast.

undifferentiated broadleaf forest (mature forest stage) and heathland (pioneer community stage), whose mean F-scores were 0.53 and 0.48, respectively. In contrast, undifferentiated conifers (mature forest stage) exhibit the highest mean F-score (0.97) (Appendix B Figure B.4). In general, these index values were not close to one (pixel-perfect classification of all groups). In addition to those mentioned above, another potential influencing factor could be the use of recent data following the step of photo interpretation, to classify the old data.

In 2019, 67% of the surface area of the BC was occupied by steady forest (mature forest stage), while only one third of the total surface area was covered by pioneer (16%) and open forest stages (17%). The present situation differed markedly from the landscape in 1942, where the main environment was the open forest stage (42%), followed closely by the mature forest stage (36%) and finally by the pioneer community stage (22%) (Appendix B Table B.2).

Satellite images showed that nowadays, two-thirds of the current land cover is composed of mature forest: beech forest (47%), followed by undifferentiated broadleaf forest (12%) and undifferentiated coniferous forest (8%) (Appendix B Table B.3, Appendix C). Overall, the proportion of the mature forest stage increased from 1942 to 2019, unlike the other stages (Fig. 4B). Nevertheless, these trends were not consistent throughout the study period. The proportion of mature forest stage first increased but then reached a plateau from 1970 to 1989, before increasing again regularly until 2019. The open forest stage decreased from 1942 to 1970, and then fluctuated as follows: increase from 1970 to 1989, decrease from 1989 until 2003, increase from 2003 to 2011 and decrease again until 2019. In a complementary way, the pioneer community stage rose slightly from 1942 to 1962, before dropping to 1989, increasing again to 2001, decreasing weakly to 2003, and increasing again to 2019. The behaviours of the pioneer and open forest stages were antagonistic, showing opposite trends (Fig. 4B), while the mature forest stage followed an independent and overall increasing pattern.

By focusing on a specific area, we can identify local changes in the land cover, due to abandoned lands or other disturbances.

In the north-western part of the BC, grasslands and heathlands are surrounded by dense beech forest (Fig. 1). This area has continuously changed, from a dominant mature forest stage in 1989 to heavy deforestation till 2011. It was then only gradually recolonised by forest until 2019. Likewise, the north-eastern part of the catchment is very heterogeneous in time and space, with a changing vegetation cover type over time (Fig. 3).

In the southwest of the basin, an increase in the mature forest stage emerged between 1942 and 1989, and contributed to a relative global increase of + 13% (from 36% in 1942 to 49% in 1989). Conversely, the pioneer community stage gradually decreased by −14% (Appendix B Table B.2). In this area, an expansion of the mature forest stage was visible between the years 2011 and 2019 (Fig. 3, Fig. 4B), as evidenced by the growth of the beech stand (broadleaf) (+7%, Appendix B Table B.3). This expansion was reinforced by the reduction in the open forest stage: decrease of the loose broadleaf stand (−4%) and of broadleaf copse (−6%).

In the south-east of the BC, an area covered by coniferous stands (mature forest stage, Fig. 1) underwent strong changes between 1970 and 1979 (Fig. 3, Appendix B Figure B.2), and then remained homogeneous from 2001 to 2019 (mean surface of 1.0 ± 0.1 Km^2). Meanwhile during this period, the pioneer community stage was more or less stable as the grassland decreased (-4%), while heathland tended to increase (+5%) (Appendix B Table B4).

3.2. Hydrochemical composition of the Baget stream water

The major hydrochemical ions (Ca^{2+}, Mg^{2+} and HCO_3^-) are reported for the period 1979–2020 in Appendix B Table B.4, while the complete hydrochemical parameters (all major element concentrations) are stated for the period 1995–2020 in Appendix B Table B.5.

As indicated by their mean concentration, the most abundant cation was Ca^{2+} (1515 ± 91 µmol.L^{-1}), followed by Mg^{2+} (171 ± 28 µmol.L^{-1}) and Na^+ and K^+ (<42 µmol.L^{-1}). The mean Ca^{2+}/Mg^{2+} molar ratio was 8.5 ± 1.2. The most abundant anion was HCO_3^- (3095 ± 233 µmol.L^{-1}), followed by SO_4^{2-} (105 ± 70 µmol.L^{-1}) and Cl^- and NO_3^- (<48 µmol.L^{-1}).

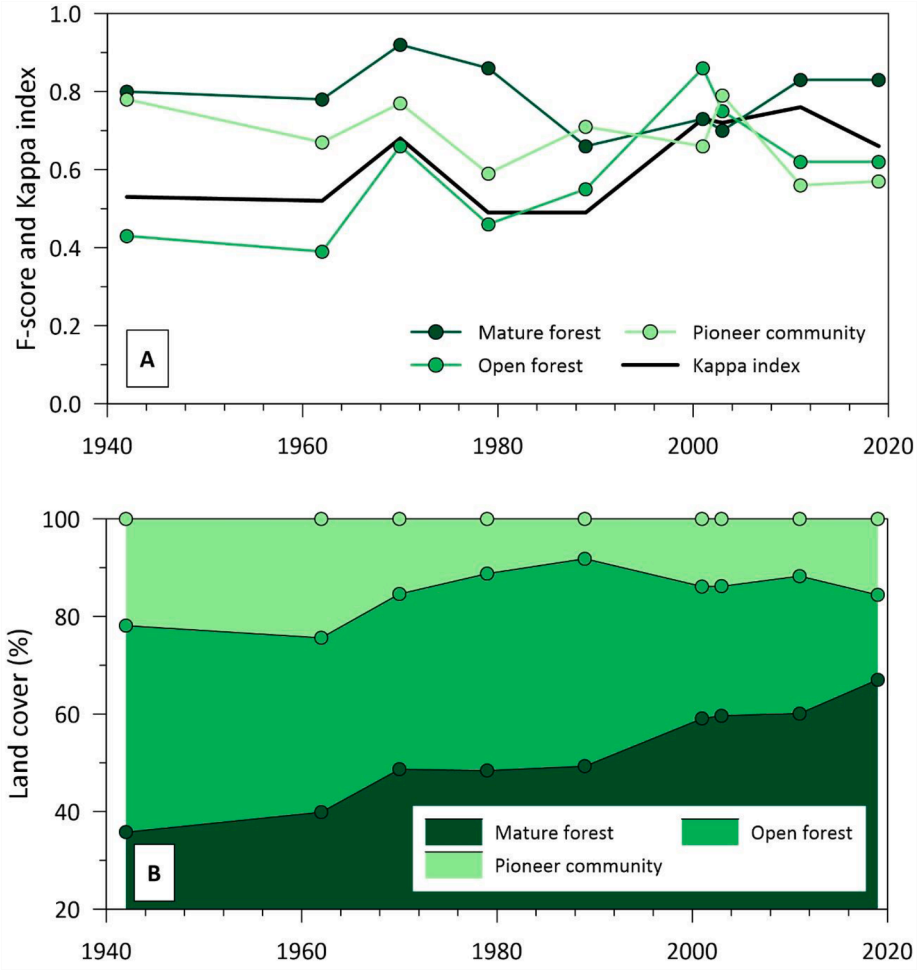

Fig. 4. (A) Evaluation (F-score and Kappa index) and (B) surface evolution of each landscape group, using aerial photographs from 1942 to 1989 and satellite imagery from 2001 to 2019.

The mean SO_4^{2-}/ HCO_3^- molar ratio was 0.05 ± 0.03. This is consistent with the results of Ulloa-Cedamanos et al. (2020) for a less extended period (1995–2018).

The two most abundant ions (Ca^{2+} and HCO_3^-) accounted on average for 89.1 ± 2.7% of instantaneous TDS ($mg.L^{-1}$) and they dominate the charge balance (mean interannual value of 98.3 ± 0.1% and of 88.0 ± 1.5% of the total sum of cations and anions in $meq.L^{-1}$, respectively (Appendix B Figure B5). The highest coefficient of variation (CV, Appendix B Table B5) of instantaneous data was for discharge (1.45) and air temperature (0.52), mainly in relation with seasonal fluctuations. The dissolved elements with the highest CV were SO_4^{2-} (0.44) and DOC (0.53), while the lowest CV were for Ca^{2+} (0.06), HCO_3^- (0.08) and TDS (0.06).

3.3. Long-term trends in stream water chemistry and landscape

At the outlet of the BC, carbonate dissolution dominate the water chemistry, accounting for 73% of TDS, followed by silicate weathering (16%) (Ulloa-Cedamanos et al., 2021b). A first analysis of long-term trends in air temperature, (Ca^{2+} + Mg^{2+}) and HCO_3^- concentrations indicated a slight increase between 1979 and 2018. In contrast, long-term trends in discharge and calculated pCO_2 in the streamwater, after degassing of CO_2 and/or calcite precipitation (Ulloa-Cedamanos et al., 2021b), did not show any significant trends (Ulloa-Cedamanos et al., 2020).

The hydrochemical dataset between 2007 and 2016 (N = 35) included only a small number of samples per year compared to the rest of the other years (mean of 53 samples per year). However, this period was considered in the long-term trend analysis because it does not modify the trends, but it takes into account a greater dispersion of the points between 2007 and 2016 (Fig. 5A and 5B). The trend of the mean annual concentrations of (Ca^{2+}+Mg^{2+}) and HCO_3^- confirmed the overall increasing trend already observed on instantaneous data by Ulloa-Cedamanos et al. (2020) ($p = 0.02$, Fig. 5A and $p < 0.01$, Fig. 5B, respectively). The lineal regression indicated a steeper slope for HCO_3^- (slope = 0.010) than for Ca^{2+} + Mg^{2+} (slope = 0.005). The annual concentration averages showed a strong significant increase ($p < 0.01$) until 2003 (increase of the slope to 0.010 for Ca^{2+}+$Mg^{2+}$and 0.014 for HCO_3^-). After this year, a decrease in concentrations was observed between 2004 and 2006, with concentrations slightly lower than those of the last 4 years of study (2017–2020). The air temperature was the only parameter showing a constant increasing trend for all the period ($p < 0.01$, Fig. 5C). Conversely, annual discharge varied around the mean with no significant trend ($p = 0.78$, Fig. 5D) during the same period. An alternation of wet and dry periods was observed on the inter-annual year variation. An increase in the stream discharge was observed for three years (2013, 2014 and 2018). This may however have led only a minor dilution effect because even for these years, concentrations of Ca^{2+}+Mg^{2+} and HCO_3^- continued to increase. Nevertheless, if we consider the measurements before 2013, the discharge trend displayed a significant decrease ($p = 0.04$) (Fig. 6).

In parallel, the trends in landscape surface for the three types of vegetation classes were quantified between 1942 and 2019 (Fig. 5D). The mature forest stage showed a regular increase from 1942 to 2019

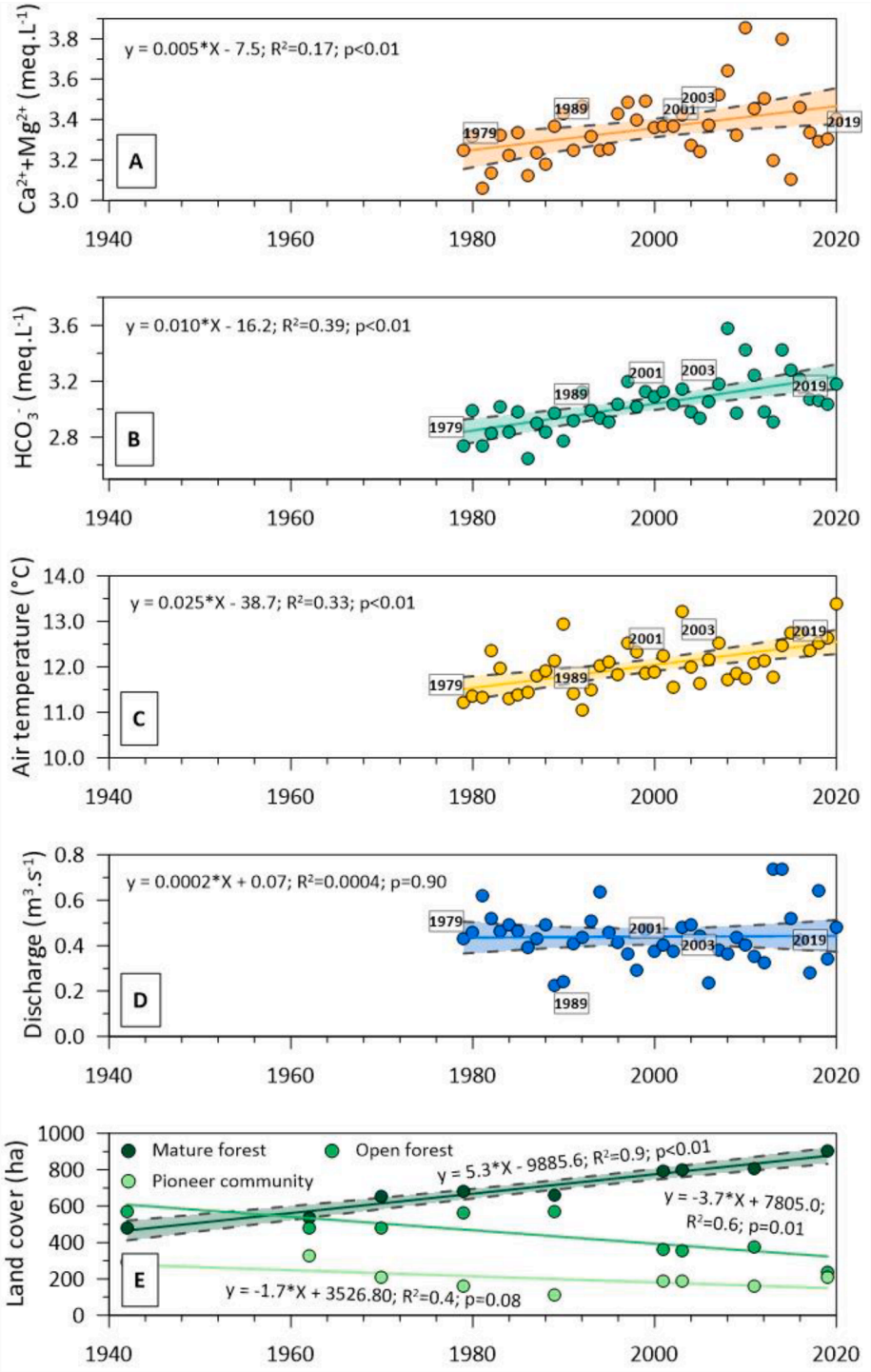

Fig. 5. Evolution of the mean annual water chemistry based on instantaneous data (A: Ca^{2+}+ Mg^{2+} and B: HCO_3^-), of mean annual hydroclimatic parameters (based on daily air temperature (C) and daily discharge (D) and of landcover transition (E). Continuous lines and surface included within dash lines represent the linear regressions and the 95% confidence interval of the long-term trends, respectively. p-value: significance level, R^2: Spearman correlation coefficient.

(R^2 = 0.9), unlike the pioneer community stage (R^2 = 0.4; mainly between 1972 and 1989, Fig. 4A) and the open forest stage (R^2 = 0.6, mainly between 1989 and 2019, Fig. 4A), which displayed an overall decrease. In addition, even if the trend was downwards for pioneer and open forest stage, their internal variations were mutually antagonistic (Fig. 5D). Indeed, it can be noticed that the observed trends for stream water chemistry, temperature and discharge have remained similar if we only consider the years concerned by the landscape transition analysis, i.e., the years 1979, 1989, 2001 and 2019.

3.4. Link between environmental indicators and stream water chemistry

The cause-effect relationship between environmental parameters and water chemical composition was investigated using the Redundancy analysis (RDA, Fig. 7). This statistical method, widely used in ecology, analyses many individual characteristics and environmental predictors simultaneously (Forester et al., 2018; Jalal et al., 2005; Sytiuk et al., 2020). According to the statistical analysis, significance (p-value) of each explanatory variable included in the RDA was tested using 1000

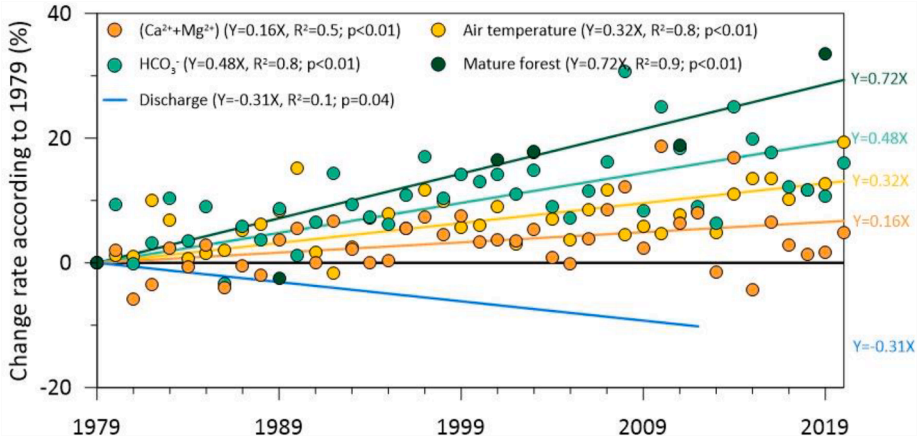

Fig. 6. Rate of change in hydrochemical and environmental indicators (in %) with reference to the year 1979 (§ Equations (4)–(6)). For discharge, only the linear regression was plotted until 2012 due to the strong dispersion of the data.

permutations.

The first RDA was computed using the instantaneous values to highlight the seasonal control of discharge and temperature on the dynamics of major elements in streamwater (Fig. 7A, N = 1685 samples). The second one was performed using the annual mean values of the previous parameters and the surface of the mature forest community, to understand their long-term cause-effect relationship on water chemistry (Fig. 7B, N = 31 years). The mature forest stage surface was chosen as an environmental indicator to complement the RDA analysis since (1) it enabled the strongest indirect relationship with the increase in soil pCO_2 (Calmels et al., 2014; Ek and Godissart, 2014) and (2) it showed the most robust performances (0.66 < F-score < 0.92) in the landscape classification model (Appendix B Table B.2 and B.3).

The first biplot (Fig. 7A, significance level of the model "p" < 0.01) involved two axes, representing 5.2% (p of the axis < 0.01) and 1% (p of the axis < 0.01) of the variance. This RDA contrasted air temperature and Mg^{2+} concentration on the upper positive side, while discharge, Ca^{2+} and HCO_3^- concentrations were positioned on the lower negative side.

The second biplot (Fig. 7B, p-value = 0.015) was composed of two axes that explained 23% (p of the axis < 0.05) and 2.7% of the variance. In this RDA, a similar pattern, which opposed air temperature to discharge on one side, and Ca^{2+} and HCO_3^- to Mg^{2+} concentrations on the other, was observed. However, Ca and HCO_3 were more closely associated to air temperature. The changes in mature forest stage and the air temperature were close and positively linked to the Ca^{2+} and HCO_3^- concentrations, in opposition to discharge.

4. Discussion

4.1. Reasons for long and short-term changes in the landscape of the Baget catchment

The surfaces of the three groups of landscape undergo successive growths and declines (Fig. 4A). However, the landscape evolution between 1942 and 2019 indicated a progressive vegetation transition towards the forest stage in the BC (Fig. 5E). This forest recolonisation was related to a decrease in the pioneer and open forest stage (Fig. 4B). In the sixties, there were 50 farming families in the catchment, while nowadays there are only 14, of which only eight live in the catchment. This is why the landscape for livestock and agriculture (grassland and heathland) was progressively abandoned and overgrown around the 1980 s, but has been re-occupied since 2000, resulting in a limited landscape opening (Fig. 4B, Fig. 5E). The example of the north-western part of the BC, with a pioneer community stage surrounded by a dense beech forest (Fig. 3), is also illustrative of this human pressure. This area which showed a near-enclosing of the landscape in 1989, was re-opened artificially before 2001 due to the construction of an access road. That is why we observed an increase in the pioneer community stage, which gradually enclosed again until 2019. The enclosing of the landscape, in response to agricultural and pastoral abandonment in mountain environments, has already been identified in other studies concerning remote areas (Chassany, 1999; Houet et al., 2012), such as the Pyrenees mountains and the Massif Central in France since the 1940s (Houet et al., 2012; Robert, 2016). Consistently, the major origin of landscape evolution in the Baget catchment was linked to the intensity of human pressure.

This is evidenced by the complementary patterns observed between the pioneer and open forest stages (Fig. 4B, Fig. 5E). Before 1989, forest recolonisation due to the abandonment of agriculture and livestock farming led first to a slight increase in open forest stage to the detriment of pioneer communities. Then from the 2000 onwards, the reuse of land for agriculture reduced the landscape area occupied by open forest stage, as these lands are quicker and easier for farmers to deforest.

The indicator of forest recolonisation tended to increase steadily but slowly (Fig. 6), as the dynamics of establishment and growth of a forest stand extend over several decades. However, locally, the razing of broadleaf stands (beech and chestnut trees) as in the south-eastern BC prior to 1979 (Fig. 3, Appendix B Figure B.2) halted this process. This area is currently occupied by coniferous stands planted after 1979 (Fig. 1, 8% of the current area of BC). Consequently, these local disturbances impacted the general trends and explain the stability of the mature forest stage observed between 1970 and 1989 (Fig. 4B, Fig. 5E).

4.2. Cause-effect relationship between environmental changes and trends in water chemistry

In this study, the main target was to determine the effect of environmental variables on the chemical composition of surface waters.

The relationships between water chemistry and environmental indicators vary depending on the temporal scale of the study. The seasonal control of temperature and discharge on the carbonate dissolution products was demonstrated using the instantaneous values (N = 1685 samples, Fig. 7A). The increase in carbonate dissolution during winter explains why Ca^{2+} and HCO_3^- show the opposite trend to temperature and in the same direction of discharge over axis 1. This is also confirmed by the systematically higher contribution of carbonate ions to the total dissolved solids (TDS) in winter (Ulloa-Cedamanos et al., 2021b). Conversely, the opposite position of Mg^{2+} (Fig. 7), originating from the dissolution of dolomite, was not surprising since its relative contribution to streamwater composition is higher during the summer low water flow period. During this period, some tributaries dry up completely, which

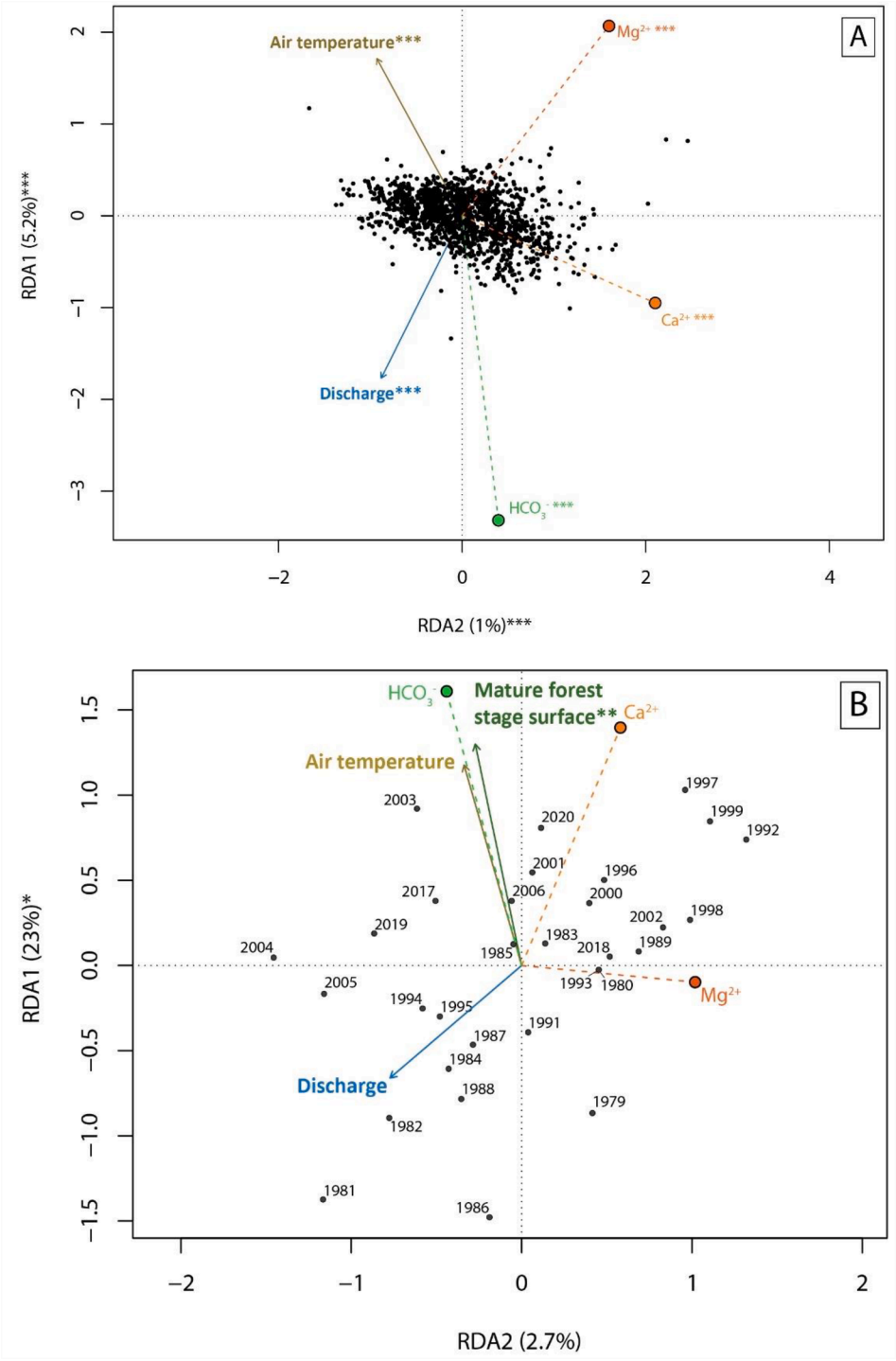

Fig. 7. (A) Redundancy analysis (RDA, N = 1685 samples, Appendix B Table B.4) of instantaneous streamwater chemical composition (meq.L^{-1}) as a function of air temperature (°C) and discharge ($m^3.s^{-1}$). (B) RDA (N = 31 years) of mean annual chemical composition of streamwater as a function of air temperature (°C), mature forest stage surface (ha) and discharge ($m^3.s^{-1}$) at the outlet of BC. Code meanings: "***" (p-value ≤ 0.001), "**" (p-value ≤ 0.01), "*" (p-value ≤ 0.05).

leads to an increased relative contribution of dissolved elements to the streamwater from certain areas. This is the case for Mg^{2+} whose contribution increased by about 10% (Ulloa-Cedamanos et al., 2020).

The landscape classification aimed to create an efficient indicator that illustrated the influence of the different land covers on the observed changes in water chemistry, expressed by the variations in (Ca^{2+} + Mg^{2+}) and HCO_3^-. The significant increase in air temperature (global warming) was identified as a key factor which might explain the significant increasing trends observed for these ions (Binet et al., 2020; Ulloa-Cedamanos et al., 2020). Except for discharge, however, no other environmental parameter supported this hypothesis. An increase in air temperature and CO_2 concentration in the atmosphere has several environmental consequences. It favours forest growth (Morison and Lawlor, 1999; Went, 1953), promoting the evapotranspiration process and hence, the uptake of soil water (Jaramillo and Destouni, 2015; Leng et al., 2015; Lippmann et al., 2019). The extent of this change can be proved and quantified by comparing the trends in precipitation (P), discharge (Q), and evapotranspiration (ET), noticeably during the

growing season (interannual monthly means from April to July, Appendix B Figure B.6) in BC. The increasing ET with the increasing proportion of forest area over the period resulted in an increasing disproportion between precipitation and discharge (P-Q) of 3.6 mm.yr^{-1} at BC (Fig. 1A), while the potential ET (ETP model) increased only by 1.8 mm.yr^{-1} at the St Girons station (Appendix B Figure B.6). Thus, the increase in forest cover impacts the water balance, by reducing surface runoff through forest interception and drainage due to increasing water demand (Khorchani et al., 2021; Tormos, 2010), by enhancing the infiltration of non-consumed water through the soil, and returning most of the water to the atmosphere through transpiration (Aussenac, 1981). Afforestation also plays a buffering role by stabilizing the discharge over time at the catchment scale (Burch et al., 1987; Hlásny et al., 2015). Conversely, landscape openness leads to a significant improvement in soil water availability (Aussenac et al., 1995) and decreases ET (Khorchani et al., 2020). Our study brings additional data to support this idea, illustrated by the opposition of discharge against air temperature and the mature forest stage surface in axis 1 in Fig. 7B (significance level of the model of 0.015).

The observed decreasing trend in stream discharge could have led to a potential accretion of the dissolved ions in surface waters (Li et al., 2010; Qin et al., 2019). The concentration/discharge relationships indicated a seasonal hydrological control on concentrations, with most of the ion concentrations decreasing with the increase of discharge (particularly obvious for SO_4^{2-} in BC; Ulloa-Cedamanos et al., 2021a), because of dilution effect (Zhong et al., 2020, Zhong et al., 2017). In such karst system, the high concentration observed both during low and high discharge conditions can be ascribed to the long water transit time and to the piston effect of more concentrated waters, respectively (Ulloa-Cedamanos et al., 2021a). The interannual increasing concentrations of (Ca^{2+} + Mg^{2+}) and HCO_3^- could either result from decreasing discharge (concentration effect), or from increasing weathering rate. The opposite patterns observed in the BC between the surface of mature forest stage and the ions originated from carbonate dissolution, against the discharge, are consistent with these hypotheses (Fig. 7B). The analysis of the interannual fluxes of (Ca^{2+} + Mg^{2+}) and HCO_3^- (Appendix B Figure B.7) revealed that these trends (deviation from the mean between 109 and −96% for HCO_3^-) are more driven by the discharge (deviation between 94 and −95%) rather than by the concentration (deviation between 18 and −13% for HCO_3^-). However, at the annual scale, the discharge drives the fluxes, but not the concentrations (Appendix B Figure B.8), as it has been observed for CO_2 consumption fluxes in BC (Ulloa-Cedamanos et al, 2021b). The strong global chemostatic behaviour of Ca^{2+} and HCO_3^- concentrations with changing discharge, was already evidenced in BC (Ulloa-Cedamanos et al, 2021a), and relies on the rapid kinetic of carbonate dissolution. Therefore, the increase in (Ca^{2+} + Mg^{2+}) and HCO_3^- concentrations should be related to an increase in the weathering process by an acid source.

4.3. Cause-effect relationship between changes in acidity source and in water chemistry

The extent of forested area in catchments could also affect DOC leaching. The elevated leaching of organic acids from soils may increase rock weathering, and consequently element products concentrations such as (Ca^{2+} + Mg^{2+}) and HCO_3^- in BC. An increasing trend in DOC concentrations was observed in European northern headwater areas as well as in agricultural areas due to decreasing SO_4^{2-} deposition, climate change and changes in land use (de Wit et al., 2021; Monteith et al., 2007; Ponnou-Delaffon et al., 2019). Long-term DOC survey was not available in BC, however, in karst systems DOC concentrations and fluxes are relatively low (1.0 ± 0.6 mg.L^{-1} and 1.3 ± 0.4 t.Km^{-2}.yr^{-1} in BC, Appendix B Table B.5) compared to forested catchments (13.3 t.Km^{-2}.yr^{-1} in Korea; Yoon et al., 2010) and to peatlands (40 ± 4 t.Km^{-2}.yr^{-1} in UK; Worrall et al., 2012 and between 16.1 ± 0.4 and 34.6 ± 1.5 t.Km^{-2}.yr^{-1} in the French Pyrenean massif; Rosset et al., 2019). The mobilisation of DOC from the upper soil horizons with the increasing discharge (Ulloa-Cedamanos et al., 2021a) may thus play a limited seasonal role in rock weathering, and its impact on interannual evolution remains unlikely in such buffered carbonate systems. The low absolute mean value of NICB (1.4 ± 1.5%, N = 855) also evidenced a good equilibrium between cation and anion charges, and consequently confirmed that the contribution of organic anions to the anionic charge remain negligible.

Under forest, litterfall and humus are enhanced. Even if organic matter (OM) storage is a slow process following land abandonment, increasing forest cover leads to higher OM in soils and evidenced a microbial origin (Nadal-Romero et al., 2021). The higher air temperature stimulates microbial activity and the decomposition of organic matter (Zhong et al., 2018). The consequent increase in CO_2 production in soil (Equation (1)) (Zeng et al., 2021; Zhao et al., 2019) contributes to accelerating the dissolution of carbonates (Equations (2) and (3)), even if the calcite solubility decreases when temperature increases (Cao et al., 2012; Plummer and Busenberg, 1982). This is consistent with the position of Ca^{2+} and HCO_3^- on axis 1 (Fig. 7B), i.e. close to air temperature and mature forest stage surface. As mentioned above, the enclosing of the landscape increases the release of organic matter into the soil, which is oxidized to produce CO_2 and then converted to carbonic acid (H_2CO_3). This weak acid weathers rocks, such as limestone, composed of mineral calcite ($CaCO_3$). Thus, the enhanced relative dissolution increases the Ca^{2+} and HCO_3^- concentrations observed in BC surface waters.

The less steep net increase of Ca^{2+}+Mg^{2+} than the net HCO_3^- increase could result from decreasing terrestrial Ca export together with decreasing SO_4^{2-} leaching (-4 µeq.L^{-1}.yr^{-1}, Fig. 8A) due to decreasing atmospheric sulfuric acid deposition or farmland NPK-fertilizers (Binet et al., 2020; Kopáček et al., 2020; Weyhenmeyer et al., 2019). The BC is characterized by a limited and sparse agricultural activity, suggesting that the external source of SO_4^{2-} must almost only be remote atmospheric deposition, which, in this mountainous area, was estimated to be lower than in the northern part of France and Europe (Pascaud et al., 2016). This hypothesis was reinforced by the interannual decrease of: (i) the contribution of the annual average SO_4^{2-} concentration to the anionic charge for HCO_3^- (Appendix B Figure B.5), and (ii) the mean annual loss of alkalinity (Fig. 8B, Equation (8)). The loss of alkalinity could be linked to the dissolution of gypsum and/or rock weathering by strong acids (H_2SO_4 and HNO_3) (Perrin et al., 2008; Ulloa-Cedamanos et al., 2020). Low and high-water level conditions caused changes in gypsum dissolution and pyrite oxidation, leading to seasonal changes of the loss of alkalinity in the BC (Fig. 8B) (Ulloa-Cedamanos et al., 2020). The interannual average of alkalinity loss decreases, with higher values before 2000 (Fig. 8B). This decrease can be explained by the decline in acid deposition from long-range atmospheric pollution, as previously shown by Binet et al. (2020) and Ulloa-Cedamanos et al. (2020) in this remote basin.

In BC, the Ca^{2+} also partly originates from the dissolution of gypsum ($CaSO_4{\cdot}2H_2O$), which accounts only for up to 4.9% of annual TDS (Ulloa-Cedamanos et al., 2021b). The decrease in water drainage in the catchment may decrease the Ca^{2+} production from the gypsum dissolution that could also contribute to the less steep net increase of Ca^{2+}+Mg^{2+} compared to the HCO_3^-.

Furthermore, because of forest recolonization, the nutrient consumption by young trees increases since they draw on the available nutrients to ensure their growth. Calcium is essential for the metabolic development of plants, while Mg^{2+} is a necessary component of chlorophyll, and therefore of photosynthesis (Bohn et al., 2004; Hepler, 2005). However, the Ca^{2+} + Mg^{2+} uptake is compensated for an equivalent release of H^+ ions that neutralize an equivalent amount of HCO_3^-. As a result, the retention of these nutrients linked to afforestation contributes to a concentration decrease of these ions, but does not change the (Ca^{2+} + Mg^{2+})/HCO_3^- ratio in stream water.

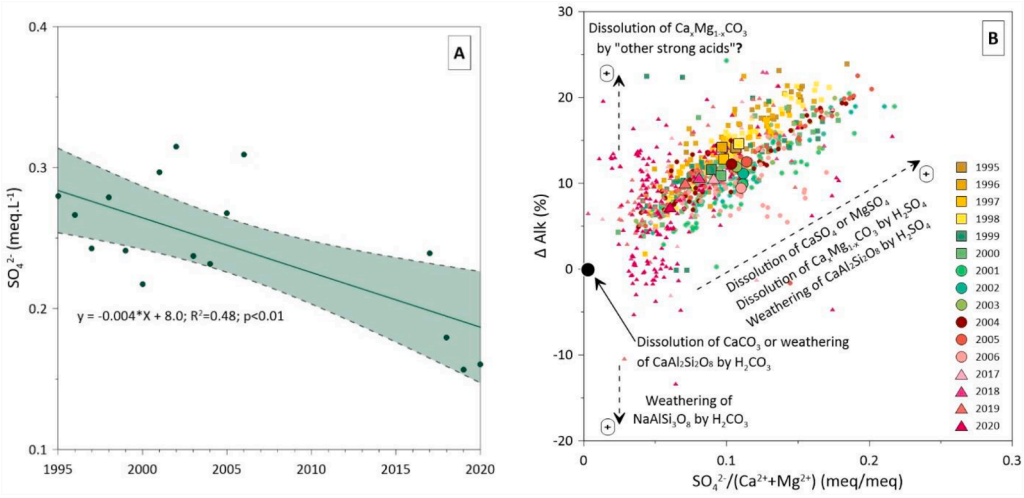

Fig. 8. (A) Evolution of the mean annual concentration of SO_4^{2-}). Continuous lines and surface included within dash lines represent the linear regression and the 95% confidence interval, respectively. (B) Relationship between ΔAlk and the ratio $SO_4^{2-}/(Ca^{2+} + Mg^{2+})$. The black lines show the main weathering processes that control the chemical composition of stream water.

5. Conclusions

This study investigated the impact of landscape changes over decades on the stream water chemistry in a small forested karst catchment from the Pyrenees Mountains, using a unique 40-year survey dataset. The method developed may it possible to harmonize heterogeneous data sources (aerial photographs from 1942 to 1989, satellite images from 2001 to 2019 and other exogenous data) to reconstruct and quantify the landscape changes undergone in the Baget catchment (BC) from 1942 to 2019. The landscape classification was split into three main classes (pioneer community, open forest and mature forest stage) to create an indicator that allowed the comparison/harmonization between aerial photographs and satellite image data, as well as to be consistent with the objectives of the study.

From 1942 to 2019, the Baget catchment has undergone a progressive enclosing of the landscape through afforestation of abandoned lands and forest growth. This change was not linear, with periods of openness, for instance, for pastoral uses. Between 1942 and 1979, the enclosing of the landscape increased due to the marked abandonment of the territory by farmers. In 1989, the area of the open forest stage decreased slightly due to the cutting of a broadleaf stand and the replanting of coniferous stands in the southeast part of BC. Then, from 1990 to 2003, we observed a re-opening of the landscape, linked to a resurgence of pastoral activities. Finally, from 2003 to 2019, the enclosing of the landscape was marked, particularly through the significant expansion of the beech stand.

The increasing forest recolonisation has an impact on the chemical composition of streamwater at the scale of this karstic catchment. Significant increasing trends ($p < 0.02$) of carbonate dissolution products, i.e., Ca^{2+}, Mg^{2+} and HCO_3^-, were observed. Changes in landscape have a delayed effect on water characteristics and chemical composition through enhanced hydrological and biogeochemical processes, such as evapotranspiration, water infiltration and rock weathering. A first indirect indicator was the decrease in the discharge due to the enclosing of the landscape and increasing water demand, which could increase the concentration effect of the dissolved elements in the water. The second indicator was the extension of forest stands, which are mainly composed of broadleaf at different phenotypic stages, and conifers (8%), which contributes to increase organic matter content in the soils. A third indicator was the increase in the average air temperature due to global climate change. This increase stimulated forest growth, enhanced the mineralization of organic matter, increasing the concentration of CO_2 in soils and consequently, the production of carbonic acid. This natural acid weathered carbonate rocks, releasing Ca^{2+}, Mg^{2+} and HCO_3^- into stream water. A fourth indicator was the decrease of SO_4^{2-} leaching, resulting in a less steep net increase in Ca^{2+} concentrations (associated with both SO_4^{2-} and HCO_3^-) than the net HCO_3^-increase (associated only with the $CaCO_3$ dissolution). Finally, we concluded that the increase in Ca + Mg (+5 μeq.L^{-1}.yr^{-1}) and alkalinity (+10 μeq.L^{-1}.yr^{-1}) in the BC stream water over the last 40 years is statistically linked to the increase in air temperature (+0.03 °C.yr^{-1}), to the enclosing of the landscape (recovery of the forest cover by + 0.05 Km^2.yr^{-1}), to the decreasing atmospheric SO_4^{2-} deposition (-4 μeq.L^{-1}.yr^{-1}), and to a lesser extent, to the decrease in discharge (-4 L.s^{-1}.yr^{-1}).

This study has demonstrated the powerful indicator of linking the historical evolution of the landscape, quantified using images, to the observed trends in the hydrochemical composition of stream waters, to highlight the internal processes of the critical zone. However, because of nested effects, it still remains a challenge to strictly quantify their respective impact on water chemical composition.

Funding

This research was supported by the CNRS-INSU (France) within the framework of the SNO Karst and IR OZCAR and by the CNRS-INEE (France) within the framework of the LTSER Zone Atelier Pyrenees-Garonne (LTSER ZA PYGAR), which is part of the IR RZA. The Eva Vrech's internship was supported by the LTSER ZA PYGAR-INEE-CNRS.

CRediT authorship contribution statement

F. Ulloa-Cedamanos: Conceptualization, Methodology, Validation, Formal analysis, Investigation, Resources, Data curation, Writing – original draft, Visualization. **J.L. Probst:** Conceptualization, Methodology, Validation, Writing – review & editing, Supervision, Project administration, Funding acquisition. **C. Marais-Sicre:** Conceptualization, Methodology, Validation, Investigation, Writing – review & editing, Supervision. **E. Vrech:** Methodology, Formal analysis, Resources, Data curation, Visualization. **E. Maire:** Conceptualization, Methodology, Validation, Resources, Data curation. **A. Probst:** Conceptualization, Methodology, Validation, Investigation, Writing – review & editing, Supervision, Project administration, Funding acquisition.

Declaration of Competing Interest

The authors declare that they have no known competing financial

interests or personal relationships that could have appeared to influence the work reported in this study.

Acknowledgments

The BC belongs to the French Karst Network (SNO Karst, Jourde et al., 2018; www.sokarst.org) initiative of the INSU/CNRS (France), which aims to strengthen knowledge-sharing and to promote cross-disciplinary research on karst systems. It is one of the observatories of the French Research Infrastructure called OZCAR (the French network of Critical Zone Observatories, (Gaillardet et al., 2018)) and also a LTSER (Long-Term Socio-Ecological Research) research site of the CNRS, France (National Centre for Scientific Research) collaborative research platform called "Zone Atelier Pyrénées-Garonne (ZA PYGAR)", which is a French Research Infrastructure called RZA (Réseau des Zones Ateliers, (Bretagnolle et al., 2019). RZA grouped with OZCAR is the French contribution to the European Research Infrastructure eLTER (Long-Term Ecosystem in Europe, (Mirtl et al., 2018). The authors specially thank the support from CNRS INEE and INSU (France), SNO KARST (INSU/CNRS, France), OZCAR and Zone Atelier Pyrénées-Garonne (LTSER ZA PYGAR).

The analytical platforms, PAPC (F. Julien, V. Payre-Suc, D. Lambrigot, and W. Amblas) at Laboratory of Functional Ecology and Environment, and the chemical lab service from the GET (C. Causserand and P. Besson) are thanked for their contribution to the analytical work during the more recent years. F. Ulloa-Cedamanos's PhD was supported by a fellowship from the French Ministry of Higher Education, Research and Innovation. Special thanks are given to Thierry Camboulive, Virginie Payre-Suc, Corinne Pautot, Franck Granouillac for their help in the field samplings and/or lab works.

The reviewers are particularly thanked for their valuable inputs, which help to improve the clarity of the manuscript.

Appendix A. Supplementary data

Supplementary data to this article can be found online at https://doi.org/10.1016/j.ecolind.2022.109023.

References

ADES database, 2021. Point d'eau BSS002MAYC (10734X0010/HY) BAGET. URL https://ades.eaufrance.fr/Fiche/PtEau?Code=10734X0010/HY (accessed 6.3.21).

Amblar-Francés, M.P., Ramos-Calzado, P., Sanchis-Lladó, J., Hernanz-Lázaro, A., Peral-García, M.C., Navascués, B., Dominguez-Alonso, M., Pastor-Saavedra, M.A., Rodríguez-Camino, E., 2020. High resolution climate change projections for the Pyrenees region, in: Advances in Science and Research. Copernicus GmbH, pp. 191–208. https://doi.org/10.5194/asr-17-191-2020.

Arrouays, D., Deslais, W., Badeau, V., 2001. The carbon content of topsoil and its geographical distribution in France. Soil Use Manag. 17, 7–11. https://doi.org/10.1079/SUM200053.

Aussenac, G., 1981. L'interception des précipitations par les peuplements forestiers. La Houille Blanche 67 (7-8), 531–536.

Aussenac, G., Granier, A., Bréda, N., 1995. Effets des modifications de la structure du couvert forestier sur le bilan hydrique, l'état hydrique des arbres et la croissance. Revue Forestière Française (1), 54.

Bakalowicz, M., 2005. Karst groundwater: A challenge for new resources. Hydrogeol. J. 13, 148–160. https://doi.org/10.1007/s10040-004-0402-9.

Bakalowicz, M., 1979. Contribution de la géochimie des eaux à la connaissance de l'aquifère karstique et de la karstification. University Pierre et Marie Curie, Paris, France.

Banque Hydro, 2021. O0485110 Le Lachein à Balaguères [Baget - Las Hountas]. URL http://www.hydro.eaufrance.fr/ (accessed 6.18.21).

Barrué-Pastor, M., Fournié, V., 1996. La montagne ariégeoise entre friche et paysage : un consensus illusoire ? Études Rurales 141, 109–123. https://doi.org/10.3406/rural.1996.3555.

Binet, S., Probst, J.L., Batiot, C., Seidel, J.L., Emblanch, C., Peyraube, N., Charlier, J.-B., Bakalowicz, M., Probst, A., 2020. Global warming and acid atmospheric deposition impacts on carbonate dissolution and CO_2 fluxes in French karst hydrosystems: evidence from hydrochemical monitoring in recent decades. Geochim. Cosmochim. Acta 270, 184–200. https://doi.org/10.1016/J.GCA.2019.11.021.

Bohn, T., Walczyk, T., Leisibach, S., Hurrell, R.F., 2004. Chlorophyll-bound Magnesium in Commonly Consumed Vegetables and Fruits: Relevance to Magnesium Nutrition. J. Food Sci. 69, S347–S350. doi:10.1111/j.1365-2621.2004.tb09947.x.

Breiman, L., 2001. Random forests. Machine Learning 45, 5–32. https://doi.org/10.1201/9780429469275-8.

Bretagnolle, V., Benoit, M., Bonnefond, M., Breton, V., Church, J.M., Gaba, S., Gilbert, D., Gillet, F., Glatron, S., Guerbois, C., Lamouroux, N., Lebouvier, M., Mazé, C., Mouchel, J.M., Ouin, A., Pays, O., Piscart, C., Ragueneau, O., Servain, S., Spiegelberger, T., Fritz, H., 2019. Action-orientated research and framework: insights from the French longterm social-ecological research network. Ecol. Soc. 24 https://doi.org/10.5751/ES-10989-240310.

Burch, G.J., Bath, R.K., Moore, I.D., O'Loughlin, E.M., 1987. Comparative hydrological behaviour of forested and cleared catchments in southeastern Australia. J. Hydrol. 90, 19–42. https://doi.org/10.1016/0022-1694(87)90171-5.

Calmels, D., Gaillardet, J., François, L., 2014. Sensitivity of carbonate weathering to soil CO_2 production by biological activity along a temperate climate transect. Chem. Geol. 390, 74–86. https://doi.org/10.1016/j.chemgeo.2014.10.010.

Camacho, O., Dobremez, L., Capillon, A., 2008. Des broussailles dans les prairies alpines. Revue de géographie alpine (96-3), 77–88.

Cao, J., Yuan, D., Groves, C., Huang, F., Yang, H., Lu, Q., 2012. Carbon fluxes and sinks: the consumption of atmospheric and soil CO_2 by carbonate rock dissolution. Acta Geol. Sin. - English Edition 86, 963–972. https://doi.org/10.1111/j.1755-6724.2012.00720.x.

Cao, Y., Xuan, Y., Tang, C., Guan, S., Peng, Y., 2019. Temporary and net sinks of atmospheric CO_2 due to chemical weathering in subtropical catchment with mixing carbonate and silicate lithology. Biogeosciences 17, 3875–3890. https://doi.org/10.5194/bg-2019-310.

Catalán, N., Marcé, R., Kothawala, D.N., Tranvik, Lars, J., 2016. Organic carbon decomposition rates controlled by water retention time across inland waters. Nat. Geosci. 9, 501–504. https://doi.org/10.1038/ngeo2720.

Chassany, J.-P., 1999. Processus de déprise agricole et enjeux socio-économiques. Ingénéries - EAT 81–89.

Clark, I., Fritz, P., 1997. Environmental isotopes in hydrogeology. CRC Press/Lewis Publishers, Boca Raton, FL.

Congalton, R.G., 1991. A review of assessing the accuracy of classifications of remotely sensed data. Remote Sens. Environ. 37 (1), 35–46.

Daher, W., Pistre, S., Kneppers, A., Bakalowicz, M., Najem, W., 2011. Karst and artificial recharge: Theoretical and practical problems. A preliminary approach to artificial recharge assessment. J. Hydrol. 408, 189–202. https://doi.org/10.1016/j.jhydrol.2011.07.017.

de Wit, H.A., Stoddard, J.L., Monteith, D.T., Sample, J.E., Austnes, K., Couture, S., Fölster, J., Higgins, S.N., Houle, D., Hruška, J., Krám, P., Kopáček, J., Paterson, A.M., Valinia, S., Van Dam, H., Vuorenmaa, J., Evans, C.D., 2021. Cleaner air reveals growing influence of climate on dissolved organic carbon trends in northern headwaters. Environ. Res. Lett. 16 (10), 104009.

Debroas, E., 2009. Géologie du bassin versant du Baget (zone nord-pyrénéenne, Ariège, France): nouvelles observations et conséquences. Strata 46, 1–93.

Deines, P., 1980. Chapter 9 - The Isotopic Composition of Reduced Organic Carbon, in: Fritz, P., Fontes, J.C. (Eds.), Handbook of Environmental Isotope Geochemistry. Elsevier, pp. 329–406. doi:10.1016/b978-0-444-41780-0.50015-8.

Dusseux, P., 2014. Exploitation de séries temporelles d'images satellites à haute résolution spatiale pour le suivi des prairies en milieu agricole. Université Rennes 2, France.

Ek, C., Godissart, J., 2014. Carbon dioxide in cave air and soil air in some karstic areas of Belgium. A prospective view. Geol. Belgica 17, 102–106.

Forester, B.R., Lasky, J.R., Wagner, H.H., Urban, D.L., 2018. Comparing methods for detecting multilocus adaptation with multivariate genotype–environment associations. Mol. Ecol. 27, 2215–2233. https://doi.org/10.1111/mec.14584.

Gaillardet, J., Braud, I., Hankard, F., Anquetin, S., Bour, O., Dorfliger, N., de Dreuzy, J.R., Galle, S., Galy, C., Gogo, S., Gourcy, L., Habets, F., Laggoun, F., Longuevergne, L., le Borgne, T., Naaim-Bouvet, F., Nord, G., Simonneaux, V., Six, D., Tallec, T., Valentin, C., Abril, G., Allemand, P., Arènes, A., Arfib, B., Arnaud, L., Arnaud, N., Arnaud, P., Audry, S., Comte, V.B., Batiot, C., Battais, A., Bellot, H., Bernard, E., Bertrand, C., Bessière, H., Binet, S., Bodin, J., Bodin, X., Boithias, L., Bouchez, J., Boudevillain, B., Moussa, I.B., Branger, F., Braun, J.J., Brunet, P., Caceres, B., Calmels, D., Cappelaere, B., Celle-Jeanton, H., Chabaux, F., Chalikakis, K., Champollion, C., Copard, Y., Cotel, C., Davy, P., Deline, P., Delrieu, G., Demarty, J., Dessert, C., Dumont, M., Emblanch, C., Ezzahar, J., Estèves, M., Favier, V., Faucheux, M., Filizola, N., Flammarion, P., Floury, P., Fovet, O., Fournier, M., Francez, A.J., Gandois, L., Gascuel, C., Gayer, E., Genthon, C., Gérard, M.F., Gilbert, D., Gouttevin, I., Grippa, M., Gruau, G., Jardani, A., Jeanneau, L., Join, J.L., Jourde, H., Karbou, F., Labat, D., Lagadeuc, Y., Lajeunesse, E., Lastennet, R., Lavado, W., Lawin, E., Lebel, T., le Bouteiller, C., Legout, C., Lejeune, Y., le Meur, E., le Moigne, N., Lions, J., Lucas, A., Malet, J.P., Marais-Sicre, C., Maréchal, J.C., Marlin, C., Martin, P., Martins, J., Martinez, J.M., Massei, N., Mauclerc, A., Mazzilli, N., Molénat, J., Moreira-Turcq, P., Mougin, E., Morin, S., Ngoupayou, J.N., Panthou, G., Peugeot, C., Picard, G., Pierret, M.C., Porel, G., Probst, A., Probst, J.L., Rabatel, A., Raclot, D., Ravanel, L., Rejiba, F., René, P., Ribolzi, O., Riotte, J., Rivière, A., Robain, H., Ruiz, L., Sanchez-Perez, J.M., Santini, W., Sauvage, S., Schoeneich, P., Seidel, J.L., Sekhar, M., Sengtaheuanghoung, O., Silvera, N., Steinmann, M., Soruco, A., Tallec, G., Thibert, E., Lao, D.V., Vincent, C., Viville, D., Wagnon, P., Zitouna, R., 2018. OZCAR: The French network of critical zone observatories. Vadose Zone J. 17, 1–24. https://doi.org/10.2136/vzj2018.04.0067.

García-Ruiz, J.M., Lana-Renault, N., 2011. Hydrological and erosive consequences of farmland abandonment in Europe, with special reference to the Mediterranean region – A review. Agric. Ecosyst. Environ. 140, 317–338. https://doi.org/10.1016/J.AGEE.2011.01.003.

García-Ruiz, J.M., López-Moreno, J.I., Vicente-Serrano, S.M., Lasanta–Martínez, T., Beguería, S., 2011. Mediterranean water resources in a global change scenario. Earth Sci. Rev. 105 (3-4), 121–139. https://doi.org/10.1016/J.EARSCIREV.2011.01.006.
Génot, J.-C., Schnitzler, A., 2012. La France des friches. De la ruralité à la féralité, Matière à débattre et décider. Éditions Quæ, Versailles.
Girard, M.-C., Girard, C.-M., 2010. Traitement des données de télédétection. Environnement et ressources naturelles, Second edi. ed. Technique et ingénierie, Dunod.
Gislason, P.O., Benediktsson, J.A., Sveinsson, J.R., 2006. Random forests for land cover classification. Pattern Recogn. Lett. 27, 294–300. https://doi.org/10.1016/j.patrec.2005.08.011.
Grinand, C., Rakotomalala, F., Gond, V., Vaudry, R., Bernoux, M., Vieilledent, G., 2013. Estimating deforestation in tropical humid and dry forests in Madagascar from 2000 to 2010 using multi-date Landsat satellite images and the random forests classifier. Remote Sens. Environ. 139, 68–80. https://doi.org/10.1016/j.rse.2013.07.008.
Guerschman, J.P., Paruelo, J.M., Di Bella, C., Giallorenzi, M.C., Pacin, F., 2003. Land cover classification in the Argentine Pampas using multi-temporal Landsat TM data. Int. J. Remote Sens. 24, 3381–3402. https://doi.org/10.1080/0143116021000021288.
Haralick, R.M., Shanmugam, K., Dinstein, I., 1973. Textural features for image classification. IEEE Trans. Syst. Man. Cybern. SMC-3 (6), 610–621.
Hartmann, J., Jansen, N., Dürr, H.H., Kempe, S., Köhler, P., 2009. Global CO_2-consumption by chemical weathering: What is the contribution of highly active weathering regions? Global Planet. Change 69, 185–194. https://doi.org/10.1016/j.gloplacha.2009.07.007.
Herrault, P.-A., 2015. Extraction de fragments forestiers et caractérisation de leurs évolutions spatio-temporelles pour évaluer l'effet de l'histoire sur la biodiversité: une approche multi-sources. Université Toulouse le Mirail - Toulouse II.
Hlásny, T., Kočický, D., Maretta, M., Sitková, Z., Barka, I., Konôpka, M., Hlavatá, H., 2015. Effect of deforestation on watershed water balance: Hydrological modelling-based approach. Forestry J. 61, 89–100. https://doi.org/10.1515/forj-2015-0017.
Houet, T., Vacquié, L., Vidal, F., Galop, D., 2012. Caractérisation de la fermeture des paysages dans les Pyrénées depuis les années 1940. Application sur le Haut-Vicdessos. Sud-Ouest européen. Presses Universitaires du Mirail, pp. 41–56.
Huang, X., Zhang, L., Li, P., 2007. Classification and extraction of spatial features in urban areas using high-resolution multispectral imagery. IEEE Geosci. Remote Sens. Lett. 4, 260–264. https://doi.org/10.1109/LGRS.2006.890540.
IPCC, 2014. Climate Change 2014: Synthesis Report. Contribution of Working Groups I, II and III to the Fifth Assessment Report of the Intergovernmental Panel on Climate Change, IPCC. IPCC, Geneva, Switzerland. doi:10.1046/j.1365-2559.2002.1340a.x.
Jalal, W., Pinel-Alloul, B., Méthot, G., 2005. Mid-term study of the ecological impacts of forest fires and timber harvesting on zooplankton communities in lakes of the boreal ecozone. J. Water Sci. 18, 221–248.
Jaramillo, F., Destouni, G., 2015. Local flow regulation and irrigation raise global human water consumption and footprint. Science 350 (6265), 1248–1251.
Jari Oksanen, F. Guillaume Blanchet, Michael Friendly, Roeland Kindt, Pierre Legendre, Dan McGlinn, Peter R. Minchin, R. B. O'Hara, Gavin L. Simpson, Peter Solymos, M. Henry H. Stevens, Eduard Szoecs, Helene Wagner, 2020. vegan: Community Ecology Package.
Jeannin, P.-Y., Hessenauer, M., Malard, A., Chapuis, V., 2016. Impact of global change on karst groundwater mineralization in the Jura Mountains. Sci. Total Environ. 541, 1208–1221. https://doi.org/10.1016/J.SCITOTENV.2015.10.008.
Johannet, A., Vayssade, B., Bertin, D., 2008. Neural networks: from black box towards transparent box - application to evapotranspiration modelling. Int. J. Comput. Intelligence 4, 163–170.
Khorchani, M., Nadal-Romero, E., Lasanta, T., Tague, C., 2021. Effects of vegetation succession and shrub clearing after land abandonment on the hydrological dynamics in the Central Spanish Pyrenees. Catena (Amst) 204, 105374.
Khorchani, M., Nadal-Romero, E., Tague, C., Lasanta, T., Zabalza, J., Lana-Renault, N., Domínguez-Castro, F., Choate, J., 2020. Effects of active and passive land use management after cropland abandonment on water and vegetation dynamics in the Central Spanish Pyrenees. Science of The Total Environment 717, 137160.
Kopáček, J., Hejzlar, J., Oulehle, F., Porcal, P., Weyhenmeyer, G.A., Norton, S.A., 2020. Disruptions and re-establishment of the calcium-bicarbonate equilibrium in freshwaters. Sci. Total Environ. 743, 140626 https://doi.org/10.1016/j.scitotenv.2020.140626.
Labat, D., Ababou, R., Mangin, A., 2000. Rainfall–runoff relations for karstic springs. Part I: convolution and spectral analyses. J. Hydrol. 238, 123–148. https://doi.org/10.1016/S0022-1694(00)00321-8.
Legendre, P., Legendre, L., 2012. Numerical Ecology, third ed. Elsevier.
Leng, G., Huang, M., Tang, Q., Leung, L.R., 2015. A modeling study of irrigation effects on global surface water and groundwater resources under a changing climate. J. Adv. Model. Earth Syst. 7, 1285–1304. https://doi.org/10.1002/2015MS000437.
Li, S.-L., Liu, C.-Q., Li, J., Lang, Y.-C., Ding, H., Li, L., 2010. Geochemistry of dissolved inorganic carbon and carbonate weathering in a small typical karstic catchment of Southwest China: Isotopic and chemical constraints. Chem. Geol. 277, 301–309. https://doi.org/10.1016/J.CHEMGEO.2010.08.013.
Lippmann, R., Babben, S., Menger, A., Delker, C., Quint, M., 2019. Development of Wild and Cultivated Plants under Global Warming Conditions. Current Biology. doi:10.1016/j.cub.2019.10.016.
Littlewood, I.G., 1995. Hydrological regimes, sampling strategies, and assessment of errors in mass load estimates for United Kingdom rivers. Environ. Int. 21, 211–220. https://doi.org/10.1016/0160-4120(95)00011-9.
López-Moreno, J.I., Vicente-Serrano, S.M., Moran-Tejeda, E., Zabalza, J., Lorenzo-Lacruz, J., García-Ruiz, J.M., 2011. Impact of climate evolution and land use changes on water yield in the Ebro basin. Hydrol. Earth Syst. Sci. 15, 311–322. https://doi.org/10.5194/hess-15-311-2011.
López-Moreno, J.I., Zabalza, J., Vicente-Serrano, S.M., Revuelto, J., Gilaberte, M., Azorin-Molina, C., Morán-Tejeda, E., García-Ruiz, J.M., Tague, C., 2014. Impact of climate and land use change on water availability and reservoir management: Scenarios in the Upper Aragón River, Spanish Pyrenees. Sci. Total Environ. 493, 1222–1231. https://doi.org/10.1016/J.SCITOTENV.2013.09.031.
Maaf-IGN, 2016. Indicators for the Sustainable Management of Metropolitan French Forests, 2015 edition, Results. Paris.
Mangin, A., 1975. Contribution à l'étude hydrodynamique des aquifères karstiques (Ann. Spéléo., 1974 29: 283-332; 1974 29: 495-601; 1975 30: 21-124). Université de Dijon, Dijon, France.
Padilla, A., Pulido-Bosch, A., Mangin, A., 1994. Relative Importance of Baseflow and Quickflow from Hydrographs of Karst Spring. Ground Water 32 (2), 267–277.
Ponnou-Delaffon, V., Probst, A., Payre-Suc, V., Granouillac, F., Ferrant, S., Perrin, A.-S., Probst, J.-L., 2019. Long and short-term trends of stream hydrochemistry and high frequency surveys as indicators of the influence of climate change, agricultural practices and internal processes (Aurade agricultural catchment, SW France). Ecol. Indic. 110, 105894. https://doi.org/10.1016/j.ecolind.2019.105894.
Marais Sicre, C., Fieuzal, R., Baup, F., 2020. Contribution of multispectral (optical and radar) satellite images to the classification of agricultural surfaces. Int. J. Appl. Earth Obs. Geoinf. 84, 101972 https://doi.org/10.1016/j.jag.2019.101972.
Miranda, E., Mutiara, A.B., Ernastuti, Wibowo, W.C., 2018. Classification of Land Cover from Sentinel-2 Imagery Using Supervised Classification Technique (Preliminary Study). In: 2018 International Conference on Information Management and Technology (ICIMTech), pp. 69–74. https://doi.org/10.1109/ICIMTech.2018.8528122.
Mirtl, M.T., Borer, E., Djukic, I., Forsius, M., Haubold, H., Hugo, W., Jourdan, J., Lindenmayer, D., McDowell, W.H., Muraoka, H., Orenstein, D.E., Pauw, J.C., Peterseil, J., Shibata, H., Wohner, C., Yu, X., Haase, P., 2018. Genesis, goals and achievements of Long-Term Ecological Research at the global scale: A critical review of ILTER and future directions. Sci. Total Environ. 626, 1439–1462.
Monteith, D.T., Stoddard, J.L., Evans, C.D., de Wit, H.A., Forsius, M., Høgåsen, T., Wilander, A., Skjelkvåle, B.L., Jeffries, D.S., Vuorenmaa, J., Keller, B., Kopécek, J., Vesely, J., 2007. Dissolved organic carbon trends resulting from changes in atmospheric deposition chemistry. Nature 450, 537–540. https://doi.org/10.1038/nature06316.
Moquet, J.S., Crave, A., Viers, J., Seyler, P., Armijos, E., Bourrel, L., Chavarri, E., Lagane, C., Laraque, A., Sven, W., Casimiro, L., Pombosa, R., Noriega, L., Vera, A., Guyot, J.L., 2011. Chemical weathering and atmospheric / soil CO_2 uptake in the Andean and Foreland Amazon basins. Chem. Geol. 287, 1–26. https://doi.org/10.1016/j.chemgeo.2011.01.005.
Morison, J.I.L., Lawlor, D.W., 1999. Interactions between increasing CO_2 concentration and temperature on plant. Plant, Cell Environ. 22, 659–682.
Morán-Tejeda, E., Ceballos-Barbancho, A., Llorente-Pinto, J.M., 2010. Hydrological response of Mediterranean headwaters to climate oscillations and land-cover changes: The mountains of Duero River basin (Central Spain). Global Planet. Change 72, 39–49. https://doi.org/10.1016/J.GLOPLACHA.2010.03.003.
Nadal-Romero, E., Rubio, P., Kremyda, V., Absalah, S., Cammeraat, E., Jansen, B., Lasanta, T., 2021. Effects of agricultural land abandonment on soil organic carbon stocks and composition of soil organic matter in the Central Spanish Pyrenees. Catena (Amst) 205, 105441.
Pascaud, A., Sauvage, S., Coddeville, P., Nicolas, M., Croisé, L., Mezdour, A., Probst, A., 2016. Contrasted spatial and long-term trends in precipitation chemistry and deposition fluxes at rural stations in France. Atmos. Environ. 146, 28–43.
Pelletier, C., Valero, S., Inglada, J., Champion, N., Marais Sicre, C., Dedieu, G., 2017. Effect of training class label noise on classification performances for land cover mapping with satellite image time series. Remote Sens. 9 (2), 173.
Perrin, A.S., Probst, A., Probst, J.-L., 2008. Impact of nitrogenous fertilizers on carbonate dissolution in small agricultural catchments: Implications for weathering CO_2 uptake at regional and global scales. Geochim. Cosmochim. Acta 72, 3105–3123. https://doi.org/10.1016/j.gca.2008.04.011.
Hepler, P.K., 2005. Calcium: A Central Regulator of Plant Growth and Development. Plant Cell 17 (8), 2142–2155.
Phillips, J.M., Webb, B.W., Walling, D.E., Leeks, G.J.L., 1999. Estimating the suspended sediment loads of rivers in the LOIS study area using infrequent samples. Hydrol. Process. 13 (7), 1035–1050.
Pierret, M.-C., Cotel, S., Ackerer, P., Beaulieu, E., Benarioumlil, S., Boucher, M., Boutin, R., Chabaux, F., Delay, F., Fourtet, C., Friedmann, P., Fritz, B., Gangloff, S., Girard, J.-F., Legtchenko, A., Viville, D., Weill, S., Probst, A., 2018. The Strengbach Catchment: A Multidisciplinary Environmental Sentry for 30 Years. Vadose Zo. J. 17, 180090. doi:10.2136/vzj2018.04.0090.
Plummer, L., Busenberg, E., 1982. The solubilities of calcite, aragonite and vaterite in CO_2-H_2O solutions between 0 and 90°C, and an evaluation of the aqueous model for the system $CaCO_3$-CO_2-H_2O. Geochim. Cosmochim. 46, 1011–1040. https://doi.org/10.1016/0016-7037(82)90056-4.
Pointereau, P., Coulon, F., 2009. Abandon et artificialisation des terres agricoles. Le Courrier de l'environnement de l'INRA 57, 109–120.
Porcal, P., Dillon, P.J., Molot, L.A., Almeida, A., 2015. Temperature dependence of photodegradation of dissolved organic matter to dissolved inorganic carbon and particulate organic carbon. PLoS ONE 10 (6), e0128884. https://doi.org/10.1371/journal.pone.0128884.
Powers, D.M.W., 2011. Evaluation: from precision, recall and F-factor to ROC, informedness, markedness & correlation. J. Mach. Learn. Technol. 2, 37–63.
Rosset, T., Gandois, L., le Roux, G., Teisserenc, R., Durantez Jimenez, P., Camboulive, T., Binet, S., 2019. Peatland contribution to stream organic carbon exports from a

montane watershed. J. Geophys. Res.: Biogeosci. 124, 3448–3464. https://doi.org/10.1029/2019JG005142.
QGIS Development Team, 2021. QGIS Geographic Information System. Open Source Geospatial Foundation Project.
Qin, C., Li, S.L., Yue, F.J., Xu, S., Ding, H., 2019. Spatiotemporal variations of dissolved inorganic carbon and controlling factors in a small karstic catchment, Southwestern China. Earth Surf. Proc. Land. 44, 2423–2436. https://doi.org/10.1002/esp.4672.
R Core Team, 2021. R: A language and environment for statistical computing. R Foundation for Statistical Computing, Vienna, Austria.
Rabbinge, R., van Diepen, C.A., 2000. Changes in agriculture and land use in Europe. Eur. J. Agron. 13, 85–99. https://doi.org/10.1016/S1161-0301(00)00067-8.
Raich, J.W., Tufekcioglu, A., 2000. Vegetation and soil respiration: Correlations and controls. Biogeochemistry 48, 71–90. https://doi.org/10.1023/A:1006112000616.
Rameau, J.-C., 1999. Accrus, successions végétales et modèles de dynamique linéaire forestière. Ingénieries-EAT 33–48.
Rasse, D.P., François, L., Aubinet, M., Kowalski, A.S., Vande Walle, I., Laitat, E., Gérard, J.-C., 2001. Modelling short-term CO_2 fluxes and long-term tree growth in temperate forests with ASPECTS. Ecol. Model. 141, 35–52. https://doi.org/10.1016/S0304-3800(01)00239-3.
Raymond, P.A., Cole, J.J., 2003. Increase in the Export of Alkalinity from North America's Largest River. Science 301 (5629), 88–91.
Reynolds, C., Escobedo, F., Clerici, N., Zea-Camaño, J., 2017. Does "greening" of neotropical cities considerably mitigate carbon dioxide emissions? The case of Medellin, Colombia. Sustainability (Switzerland) 9 (5), 785.
Robert, C., 2016. Comprendre les changements d'utilisation des terres en France pour mieux estimer leurs impacts sur les émissions de gaz à effet de serre. Université Paris Denis Diderot, De l'observation à la modélisation.
Rodriguez-Galiano, V.F., Ghimire, B., Rogan, J., Chica-Olmo, M., Rigol-Sanchez, J.P., 2012. An assessment of the effectiveness of a random forest classifier for land-cover classification. ISPRS J. Photogramm. Remote Sens. 67, 93–104. https://doi.org/10.1016/j.isprsjprs.2011.11.002.
RStudio Team, 2020. RStudio: Integrated Development for R. RStudio, PBC, Boston, MA.
Sawadogo, H., Zombre, N., Bock, L., Lacroix, D., 2008. Evolution de l'occupation du sol de Ziga dans le Yatenga (Burkina Faso) à partir de photographies aériennes. Télédétection 8, 59–73.
Stets, E.G., Kelly, V.J., Crawford, C.G., 2014. Long-term trends in alkalinity in large rivers of the conterminous US in relation to acidification, agriculture, and hydrologic modification. Sci. Total Environ. 488–489, 280–289. https://doi.org/10.1016/J.SCITOTENV.2014.04.054.
Sytiuk, A., Cereghino, R., Hamard, S., Delarue, F.F., Dorrepaal, E., Kuttim, M., Lamentowicz, M., Pourrut, B., Robroek, B.J.M., Tuittila, E.-S., Jassey, V.E.J., Céréghino, R., Hamard, S., Delarue, F.F., Dorrepaal, E., Lamentowicz, M., Pourrut, B., Robroek, B.J.M., Tuittila, E.-S., Jassey, V.E.J., 2020. Morphological and biochemical responses of Sphagnum mosses to environmental changes. bioRxiv 2020.10.29.360388.
Theurillat, J.-P., Guisan, A., 2001. Potential Impact of Climate Change on Vegetation in the European Alps: A Review. Climatic Change 50, 77–109 (2001). doi:10.1023/A:1010632015572.
Tormos, T., 2010. Analyse à l'échelle régionale de l'impact de l'occupation du sol dans les corridors rivulaires sur l'état écologique des cours d'eau. AgroParisTech, France.
Ulloa-Cedamanos, F., Probst, A., Dos-Santos, V., Camboulive, T., Granouillac, F., Probst, J.-L., 2021a. Stream hydrochemical response to flood events in a multi-lithological karstic catchment from the Pyrenees Mountains (SW France). Water 13, 1818.
Ulloa-Cedamanos, F., Probst, A., Moussa, I., Probst, J.-L., 2021b. Chemical weathering and CO_2 consumption in a multi-lithological karstic critical zone: long term hydrochemical trends and isotopic survey. Chem. Geol. 585, 120567 https://doi.org/10.1016/j.chemgeo.2021.120567.
Ulloa-Cedamanos, F., Probst, J.-L., Binet, S., Camboulive, T., Payre-Suc, V., Pautot, C., Bakalowicz, M., Beranger, S., Probst, A., 2020. A forty-year karstic critical zone survey (baget catchment, pyrenees-france): Lithologic and hydroclimatic controls on seasonal and inter- annual variations of stream water chemical composition, pCO_2, and carbonate equilibrium. Water 12 (5), 1227.
Van Rijsbergen, C.J., 1979. Information Retrieval, 2nd ed. ed, Journal of the American Society for Information Science. Butterworths, London.
Vuorenmaa, J., Augustaitis, A., Beudert, B., Bochenek, W., Clarke, N., de Wit, H.A., Dirnböck, T., Frey, J., Hakola, H., Kleemola, S., Kobler, J., Krám, P., Lindroos, A.-J., Lundin, L., Löfgren, S., Marchetto, A., Pecka, T., Schulte-Bisping, H., Skotak, K., Srybny, A., Szpikowski, J., Ukonmaanaho, L., Váňa, M., Åkerblom, S., Forsius, M., 2018. Long-term changes (1990–2015) in the atmospheric deposition and runoff water chemistry of sulphate, inorganic nitrogen and acidity for forested catchments in Europe in relation to changes in emissions and hydrometeorological conditions. Sci. Total Environ. 625, 1129–1145. doi:10.1016/j.scitotenv.2017.12. 245.
Went, F.W., 1953. The effect of temperature on plant growth. Annu. Rev. Plant Physiol. 4, 347–362. https://doi.org/10.1146/annurev. pp. 04.060153.002023.
Weyhenmeyer, G.A., Hartmann, J., Hessen, D.O., Kopáček, J., Hejzlar, J., Jacquet, S., Hamilton, S.K., Verburg, P., Leach, T.H., Schmid, M., Flaim, G., Nõges, T., Nõges, P., Wentzky, V.C., Rogora, M., Rusak, J.A., Kosten, S., Paterson, A.M., Teubner, K., Higgins, S.N., Lawrence, G., Kangur, K., Kokorite, I., Cerasino, L., Funk, C., Harvey, R., Moatar, F., de Wit, H.A., Zechmeister, T., 2019. Widespread diminishing anthropogenic effects on calcium in freshwaters. Sci. Rep. 9 https://doi.org/10.1038/s41598-019-46838-w.
Worrall, F., Davies, H., Bhogal, A., Lilly, A., Evans, M., Turner, K., Burt, T., Barraclough, D., Smith, P., Merrington, G., 2012. The flux of DOC from the UK - Predicting the role of soils, land use and net watershed losses. J. Hydrol. 448–449, 149–160. https://doi.org/10.1016/j.jhydrol.2012.04.053.
Yan, J., Wang, Y.P., Zhou, G., Li, S., Yu, G., Li, K., 2011. Carbon uptake by karsts in the Houzhai Basin, southwest China. J. Geophys. Res. Biogeosci. 116 https://doi.org/10.1029/2011JG001686.
Yoon, S.W., Chung, S.W., Oh, D.G., Lee, J.W., 2010. Monitoring of non-point source pollutants load from a mixed forest land use. J. Environ. Sci. 22, 801–805. https://doi.org/10.1016/S1001-0742(09)60180-7.
Zeng, S., Liu, Z., Goldscheider, N., Frank, S., Goeppert, N., Kaufmann, G., Zeng, C., Zeng, Q., Sun, H., 2021. Comparisons on the effects of temperature, runoff, and land-cover on carbonate weathering in different karst catchments: insights into the future global carbon cycle. Hydrogeol. J. 29 (1), 331–345.
Zhao, R., Liu, Z., Huang, H., Dong, L., 2019. Difference in the relationship between soil CO_2 concentration and the karst – related carbon cycle under different land use types in southwest China. Carbonates Evaporites 34, 1569–1581. https://doi.org/10.1007/s13146-019-00506-2.
Zhong, J., Li, S.-L., Ibarra, D.E., Ding, H., Liu, C.-Q., 2020. Solute Production and Transport Processes in Chinese Monsoonal Rivers: Implications for Global Climate Change. Global Biogeochemical Cycles 34, e2020GB006541. doi:10.1029/2020GB006541.
Zhong, J., Li, S.L., Liu, J., Ding, H., Sun, X., Xu, S., Wang, T., Ellam, R.M., Liu, C.Q., 2018. Climate Variability Controls on CO_2 Consumption Fluxes and Carbon Dynamics for Monsoonal Rivers: Evidence From Xijiang River, Southwest China. J. Geophys. Res. Biogeosci. 123, 2553–2567. https://doi.org/10.1029/2018JG004439.
Zhong, J., Li, S.L., Tao, F., Yue, F., Liu, C.Q., 2017. Sensitivity of chemical weathering and dissolved carbon dynamics to hydrological conditions in a typical karst river. Sci. Rep. 7, 1–9. https://doi.org/10.1038/srep42944.